1 2 9 0

UNIVERSIDADE D
COIMBRA

Ahmad Shumayal

TRIBOCORROSION ANALYSIS OF TI6AL4V ALLOYS PRODUCED BY SELECTIVE LASER MELTING

Dissertação no âmbito do Mestrado Conjunto Europeu em Tribologia de Superfícies e Interfaces orientada pelo Professor Doutor Amílcar Ramalho e Doutor Luís Vilhena apresentada ao Departamento de Engenharia Mecânica da Faculdade de Ciências e Tecnologia da Universidade de Coimbra

Julho de 2019

FCTUC FACULDADE DE CIÊNCIAS E TECNOLOGIA
UNIVERSIDADE DE COIMBRA
rDEPARTAMENTO DE ENGENHARIA MECÂNICA

Tribocorrosion analysis of Ti6Al4V alloys produced by Selective Laser Melting

Submitted in Partial Fulfilment of the Requirements for the Degree of Master in Tribology of Surface and Interfaces

Author

Ahmad Shumayal

Advisors

Professor Amílcar Ramalho

Professor Luís Vilhena

Jury

President	Professor Bruno Trindade Associate Professor at University of Coimbra
Vowel	Professor Albano Cavaleiro Full Professor at University of Coimbra
Advisor	Professor Luís Vilhena Researcher at University of Coimbra

In the framework of Joint European Master in Tribology of Surfaces and Interfaces

tribos joint european master in tribology of surfaces and interfaces
Ljubljana • Leeds • Coimbra • Luleå

Acknowledgements

I am grateful to Professor Amílcar Ramalho and Doctor Luís Vilhena for supporting me in this work and guiding me whenever necessary. I am also grateful to the TRIBOS consortium for giving me the opportunity in this program and see it to completion.

Abstract

Titanium alloys have been utilized in various applications from Aerospace and Automobiles to their use as biomedical materials (eg. used as an implant) which is due to their high resistance of the combined wear and corrosion which could otherwise be detrimental to the lifetime of the product. Ti6Al4V, also known as Grade 5 Titanium alloy commercially, has been successfully used in biotechnology applications (e.g. cavity implants or knee joints) due to having best of both worlds (excellent mechanical characteristics and biocompatibility with suitable tribo-corrosion characteristics).

Since Ti6Al4V is used in specialized applications, by having the choice to play with the geometrical construction and control, of certain parameters like porosity, it is often tempting to produce such alloy as a 3D printed product, which not only reduces raw material used but also reduces the lead time from manufacturing to finishing.

Comparing two samples of Ti6Al4V, one produced using conventional subtractive manufacturing (machining) and another produced using additive manufacturing process - Selective Laser Melting (SLM). They were tested for electrochemically by Potentiodynamic Polarization Method, followed by Open Circuit Potential (OCP) monitoring before, after and during a tribological test against a Zirconia counter body while being submerged in artificial saliva (to mimic a dental implant) per load (3, 5 and 7 N) per sample.

The potential of the working electrode was monitored using the Open Circuit Potential (OCP) technique under simple resting conditions and with tribometer input (reciprocating sliding of ball-on-flat configuration) for different loads for the same number of cycles and frequency. Polarization curves, representing the current density (A/cm^2) vs. potential (V vs. SCE) were obtained and the corrosion resistance was compared and discussed followed by an evaluation of COF and wear.

Keywords: Tribocorrosion, Additive Manufacturing, Traditional/Conventional Manufacturing, Dental Implants.

Contents

List of Figures 1

List of Tables 3

Chapter 1 Introduction 4

1.1 Motivation 5

Chapter 2 State of Art 6

2.1 3D Printing 6

2.1.1 History 7

2.1.2 Selective Laser Melting (SLM) 11

2.1.3 Applications 12

2.2 Dental Implants 14

2.2.1 Impact of Lubrication by Saliva 14

2.2.2 Additive Manufacturing and Dental Implants 16

2.2.3 Bone Tissue Engineering (Osseointegration) 16

2.2.4 Tribology and Dental Implants 21

Chapter 3 Methodology 22

3.1 Sample Preparation 23

3.2 Electrochemical Evaluation 25

3.3 Tribometer 27

Chapter 4 Results and Discussion 29

4.1 Electrochemical Behavior 29

4.2 Effect of applied load on OCP measurements 32

4.3 Friction behaviour 36

4.4 Wear Behaviour 38

Chapter 5 Conclusions 45

List of Figures

Figure 2.1 AM Timeline [10].....24
Figure 2.2 CFM International's 3D printed fuel nozzle which reduces part count from 18 to just 1[17].....13
Figure 2.3 Example of a Dental Implant [36].....16
Figure 2.4 Bone's chemical composition, water is included under the Organic phase [38].....18
Figure 2.5 Additively Manufactured Titanium Scaffold schematic, modified by Gelatin within the pores for improving Osteogenesis [42].....19
Figure 2.6 Schematic for a Cell-based bone cell regeneration from a Titanium Alloy scaffold [42].....20
Figure 2.7 An example of tailor designing with SLM for Different Triply Periodic minimal surfaces of Ti-6Al-4V helps to suit the type of bone, since not all bones are created equal, demonstrating the dependence on Geometry and Density [54].....21
Figure 2.8 Reactive forces on a dental implant from normal functioning [58].....22
Figure 3.1 Ti6Al4V samples: (a) produced by conventional method and, (b) produced by SLM.23
Figure 3.2 (a) top view and; (b) underside of the Ti6Al4V sample to which a wire was soldered.....23
Figure 3.3 Schematic model of the setup with WE: Working Electrode, RE: Reference Electrode and CE: Counter Electrode connected to a Potentiostat with a Zirconia ball held under a Normal Load from a spring, adjustable by tightening or loosening a bolt (not shown) as appropriate to modify the compression load on spring.....26
Figure 3.4 Example of input parameters for performing Linear Polarization Resistance method.27
Figure 3.5 Experimental Setup of the Triboelectrochemical cell.....28
Figure 4.1 Potentiodynamic Polarization curves for Ti6Al4V alloy produced conventionally (orange curve) and by SLM process (blue curve). The different domains and different corrosion parameters are exemplify for the Ti6Al4V obtained by conventional process (orange).....29
Figure 4.2 More pits seen in (a) XZ plane than (b) XY plane on SLM produced Ti-6Al-4V [62]31
Figure 4.3 Schematic of (a) Laser scan direction and (b) 3D diagram of SLM produced Titanium Grade 5 [62].....31
Figure 4.4 Evolution in the OCP of the Conventional sample with time - before, during and after reciprocating sliding test for each of the loads of: 3 N, 5 N and 7 N.....33

Figure 4.5 Evolution in The OCP of the SLM sample with time - before, during and after reciprocating sliding test for each of the loads of: 3 N, 5 N and 7 N. 34
Figure 4.6 Figure 4.6 A possible schematic of the mass flow of the tribo-corrosion system [67] 35
Figure 4.7 Evolution of the COF with sliding time for: (a) Conventional sample and; (b) SLM sample 36
Figure 4.8 Steady state coefficient of friction for conventional and SLM samples for different applied loads (3 N, 5 N and 7 N). 37
Figure 4.9 Cross section profiles from the wear tracks rubbing against a Zirconia Ball under 3 N, 5 N and 7 N applied loads: (a) SLM sample; (b) Conventional sample.. 39
Figure 4.10 3D wear profiles from the wear tracks for SLM sample rubbing against a Zirconia ball under different applied loads: (c) 3 N, (d) 5 N and (e) 7N.. 40
Figure 4.11 3D wear profiles from the wear tracks for Conventional sample rubbing against a Zirconia ball under different applied loads: (c) 3 N, (d) 5 N and (e) 7 N. 41
Figure 4.12 Evolution of the wear volume vs. sliding distance times normal load for both conventional and SLM samples. 42
Figure 4.13 Example of micrograph of the Zirconia ball wear scar rubbing against Ti6Al4V (conventional produced) under 7 N applied load and 3 Hz frequency 42
Figure 4.14 Typical microstructure of Ti6Al4V produced by SLM showing the acicular α' [62] 43
Figure 4.15 SEM micrograph showing wear tracks of SLM sample with 3N of load at different magnification levels 43
Figure 4.16 SEM micrograph showing wear tracks of conventional sample with 3N of load at different magnification levels. 44
Figure 4.17 SEM micrographs in BSE mode for: (a) SLM and, (b) conventional sample. 44

List of Tables

Table 2.1 Various technologies available under two categories of AM for Titanium Alloys [11]10
Table 3.1 Chemical composition of titanium alloy Ti6Al4V by SLM [59] 24
Table 3.2 Mechanical Properties of the sample produced by SLM [59] 24
Table 3.3 The Chemical Composition of the Artificial Saliva used in the experiment (g/L).....25
Table 3.4 Reciprocating Ball on Flat configuration for the tribological experiment.....25
Table 4.1 Calculations of Corrosion Current, Corrosion Potential, ΔE and Corrosion Rate from the Potentiodynamic Polarization Curves.....32
Table 4.2 Summary of Mean Coefficient of Friction 38
Table 4.3 Wear Volumes 41

Chapter 1

Introduction

With the start of the digital age, we have brought to ourselves the age of “3D Printing” where a computer coordinates manufacturing in a way, like an ordinary Inkjet printer but over 3 dimensions instead of 2. The biggest advantage of this way of manufacturing is the efficient use of raw material for making complex shapes using fewer parts. At the same time, the cost is one of the biggest disadvantages of this technology even today since the invention in 1984 [1].

Additive Manufacturing, which can be another word for 3D Printing is a process of synthesizing 3 dimensional solid objects from a digital instruction set. The process of synthesis itself can be done in various methods which can make one different from the other. But in principle, it is always an additive process whereby the desired object is fabricated by depositing a series of successive layers to completion of manufacturing.

Given the increasing popularity of AM as a choice of manufacturing for existing products, especially the implants, it is important to understand the consequences of such a decision purely from a functional point of view. To properly investigate the effects, a certain manufacturing process can have, it is necessary to have all other variables as the same. For this reason, two sets of the same Titanium Alloy (Grade 5) samples were acquired, one produced by Selective Laser Melting (AM) and another produced by traditional subtractive manufacturing.

The effect a manufacturing process could have or not have is investigated and the implications of this are discussed for prevention or reduction of surface degradation of the given material when used as an implant.

1.1 Motivation

Titanium alloys currently dominate the market of dental implants applications since it has a comparatively low Young's modulus (close to that of cortical bone), high cyclic fatigue resistance and ability to readily form a nascent oxide layer. Titanium oxide formed naturally through exposure to aerobic environments enhances osseointegration since the mechanical strength of cP-Ti is strength-limited. This has thus seen the limited application in only specific parts where static structural demands are relatively lower such as; pacemaker, pacemaker cases, heart valve cages, hip cup shells, crowns of teeth and bridges, within-the-bone (endosseous) dental implants. Passivity is identified by a flat line in a typical linear polarization curve during the oxidation stage of the process. This passive layer, just like in the case of Aluminum, provides a good corrosion resistance as the protective oxide layer is formed. This starts to serve as a boundary between the bulk metal and the corrosive environment. However, when the surface is 'scratched' (acted upon by a counter body) this oxide layer gets broken and Titanium ions get exposed to the surrounding, which is tissues in the case of implants.

Any biological implants that are placed inside the body, it prepares to give a reaction of either acceptance or rejection. If it is accepted, the body builds up connective tissues around the implant which depends on the amount of movement, the toxicity of dissolved products and dissolution rates on neighbouring tissues [2]. If the body chooses to reject the implant, it does this by treating it as a foreign body and not one of its own. Thus, the body tries to attack it which leads to adverse inflammations. In the case of Ti6Al4V, this can get triggered when the so-called passive-oxide layer is broken and the resistance to corrosion is no longer present. Then we consider the implant to have appeared in radar for the body to treat it a foreign infection by releasing White Blood Cells (WBCs) to attack it. We do not want this to happen, therefore a combination of tribology and corrosion tests need to happen.

Since Titanium alloy (Grade 5) is already the metal of choice today for implants which also appears to be a good market for Additive Manufacturing, it is essential to understand if and how, it can affect the characteristics of the final product from a functional point of view keeping in mind the tempting benefits of AM from an efficiency and design point of view, over traditional/conventional manufacturing (reduced waste of raw material and product lead times).

Chapter 2

State of Art

Here is an outline on the basics and established facts about Additive Manufacturing, their characteristics, and types of manufacturing processes discussed in general, followed by a detailed discussion on the dental aspect of the application. The most related studies and works are discussed surrounding the topic at hand.

2.1 3D Printing

The main advent of Additive Manufacturing and 3D Printing was from the commercialization in 1987 of Stereolithography according to the Wohlers Report 2014[1] [3]. While the earliest inventions happened in the 1960s to the 1990s, it was largely the industry adoption that accelerated development and brought us big strides in the technology that we see today as can be observed from literally anything that was industrialized from Military applications to Automotive industry and software.

If the industry has a need, a lot of research and development would be done. Anything that is left untouched is probably best explained in a concise manner as the industry has little to do with it. For example, the immense development in the internal combustion engines, brakes and transmissions by the automotive industry. Nobody could have imagined a few decades ago, such efficient 4-cylinder engines, continuously varying transmissions or dual clutch transmissions easily available in the market today on road-legal cars. However, at the same time, Diesel-gate occurred and indicated the world that we have probably reached the end of pushing the frontiers on emissions and automotive diesel engines [4] [5]. Today, after the revolution (or read “competition”) brought by the Tesla car company, all traditional car brands have rushed towards electric car development for fear of losing out. Motorsport regulations continue to push boundaries in the direction of efficiency, hybridization and electric power as with the case of Formula 1 and Formula E respectively, single-handedly being responsible for a lot of Technology and Knowledge Transfer. [6].

[1] Wohlers Associates are reputed as one of the best experts globally on the past, present & future of AM operating as a consultants on Rapid Product Development [3].

While Academic Research in the traditional sense could always be at the forefront, it is only the commercialization and the industry that truly materialize an invention or gadget. Like a positive feedback system, the industry does fund a lot of research, especially if they see their benefit in it [7] [8] [9].

2.1.1 History

Additive Manufacturing is quite old today but still considered by some to be relatively new in the grand scheme of things from an implementation point of view. It is helpful to think about the object to be manufactured using this technique from the ground up across cross-sections taken at minute intervals [10].

Stereolithography has clearly played a very important role in developing the Additive Manufacturing Process with metals and plastic that we have come to know today which makes it impossible to ignore this aspect of history, no matter how unrelated it may appear to some.

The Wohler's report credits the Battelle Memorial Institute for their first try in producing solid three-dimensional objects with photopolymers as the raw material and using the laser to selectively target the substrate. This experiment utilized two intersecting beams of the laser of different frequencies in the centre of a resin vat to try and solidify/polymerize the substance at the point of convergence in the late 1960s. This very photopolymer resin was invented just a decade before by DuPont in the 1950s.

Wyn Kelly Swainson filed for a patent named "Method of Producing a 3D Figure by Holography on a similar dual laser beam approach" in 1967 from Denmark. Thereafter, they inaugurated and established a corporation called 'Formigraphic Engine Company' in the American state of California, in plans to further create and inevitably market his innovation.

In the mid-1970s, Formigraphic Engine Co. utilized the same double laser approach in the main business of their laser-prototyping venture, a procedure it has called 'photochemical machining'. In 1974, Formigraphic exhibited the synthesis of a solid article utilizing a simple but primitive system. Afterwards, Formigraphic moved towards becoming Omtec Replication, when a union was framed with the earlier mentioned Battelle Institute. Purportedly, work was yet 'in progress' even in 1994, since it never established an economically viable framework.

Dr Robert Schwerzel and Dr Vincent McGinniss, formerly with Battelle, then developed similar techniques with sponsorship from DARPA.

By the end of the 1970s, Dynell Electronics Corporation had claimed many patents on *solid photography*. This technique involved milling the cross sections by a computer like a CNC Machine or optionally, with a laser, then stacking the cross-sectional layers on top of each other to form a final product. In 1977, they had eventually merged with United Technologies Corporations which resulted in the formation of a new corporation called Solid Photography and allied with the Sculpture retail outlet which later changed its name to Robotic Vision. Solid Copier and Solid Photography then went on to function as subsidiaries for another decade.

Pursuing further history of Stereolithography techniques and even comprehensive non-SL techniques is beyond the scope of this study and the full Wohler's Associates report can be referred for more details. Further, from here, we give a cursory glance at the introduction of some key non-SL systems.

Three AM innovations out of many were popularized and commercialized from 1991 which include

1. Helisys brought Laminated Object Manufacturing (LOM) by cutting and fortifying sheet material with the assistance of a carefully guided laser guided by a computer.
2. Stratasys utilized Fused Deposition Modeling (FDM) where thermoplastic materials were extruded in a filament form to deliver parts, layer by layer.
3. Cubital utilized Solid Ground Curing (SGC) where an Ultraviolet light-sensitive liquid polymer would polymerize (making it solid) when passed through UV light over electrostatic toner masks over a glass plate.

Today, neither Helisys nor Cubital is in business. However, innovation did not stop and corporations continued to compete with various techniques and each other. They went on to introduce low-cost 3D printers from 1996 by Stratasys and around the same time, Z Corp launched their Z402 3D Printer designed for *rapid prototyping* based on MIT's inkjet printing technology labelled as 3DP. The Z402 used powders of Starch and Plaster based raw material and bound them with a water-based liquid.

After a series of paper lamination systems, AeroMet (1997-2005) started as a subsidiary of MTS Systems Corporation and started using a procedure called Laser Additive Manufacturing (LAM) which incorporated a high power laser and powdered titanium alloys as the raw mater, producing parts for the aerospace industry, providing its services as a contractor. The reason AeroMet was dissolved was blamed on the lack of profitability in the production of titanium parts for the aerospace industry through printing.

By early 2006, Stratasys signed agreements with Arcam to distribute Electron Beam Melting (EBM) systems and ended up considerably lowering down the costs of their own products.

Z Corp's zp140 and zp131 composite water-curing material could be used without any secondary coatings and with finer features for more accurate results by April 2007 where Swedish Arcam brought their huge build volume EBM machine, which was later compatible with Titanium Grade 2 material too by May 2008, while EOS launched Formiga P 100 laser sintering system. Stratasys was not to be left behind in the competition and announced their FDM 200mc machine which used ABSplus as raw material. Reactive materials (i.e., titanium and aluminium alloys) could now be processed by the Concept Laser's M2 cusing system.

For nearly every month of every year of this decade, there were various developments with resin and ABS material/polyamide over various techniques which can only be termed as fierce commercial competition.

By the end of 2010, EuroMold launched many new products. EOS inaugurated their EOSINT M 280 machine capable of running in both Nitrogen or Argon environments and

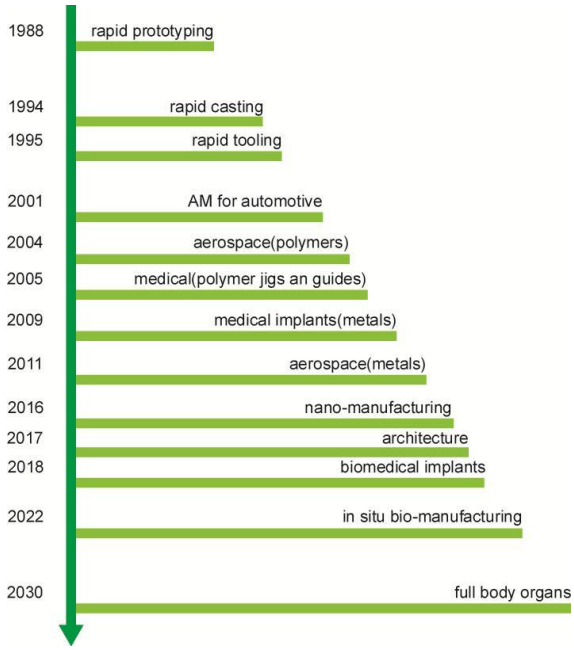

Figure 2.1 AM Timeline [10]

allowed clients to use titanium alloys, nickel alloys (IN 625) cobalt-chrome and stainless steel, together with models to work with fireproof and flexible polymers like PrimePart FR and ST respectively.

The key takeaway from this period is how swiftly the paradigm shifted from looking at AM from *Rapid Prototyping* to *Rapid Manufacturing*.

Classification

Table 2.1 Various technologies available under two categories of AM for Titanium Alloys [11]

Additive Manufacturing Category	Technology	Description
Powder Bed Fusion [PBF]	Selective Laser Sintering (SLS)	Uses laser and metal powder for sintering and bonding
	Direct Metal Laser Sintering (DMLS)	Uses laser and metal powder for sintering, melting and bonding
	Laser Melting (LM)	Uses laser and metal powder for melting and bonding
	Selective Laser Melting (SLM)	Uses laser and metal powder for melting and bonding
	LaserCUSING	Uses laser and metal powder for melting and bonding
	Electron Beam Melting (EBM)	Uses electron beam and metal powder for melting and bonding
Directed Energy Deposition [DED]	Direct Metal Deposition (DMD)	Uses laser and metal powder for melting and depositing using a patented closed-loop process
	Laser Engineered Net Shaping (LENS)	Uses laser and metal powder for melting and depositing
	Direct Manufacturing (DM)	Uses electron beam and metal wire for melting and depositing

	Shaped Metal Deposition or Wire and Arc Additive Manufacturing (WAAM)	Uses electric arc and metal wire for melting and depositing

2.1.2 Selective Laser Melting (SLM)

It was begun and patented by the Fraunhofer Institute ILT in Aachen, Germany as a basic patent DE 19649865. The researchers in *F&S Stereolithographietechnik GmbH* formed a joint partnership with ILT and eventually formed a commercial partnership with SLM Solutions GmbH.

It is also called interchangeably as Direct Metal Laser Sintering (DMLS) and Laser Powder Bed Fusion (LPBF) and sees usage in AM/3D Printing techniques for rapid prototyping or rapid manufacturing where high-power density laser is made use of, for melting and joining metallic powder particles with each other [12]. This may seem to contradict with Table 1 when one sees that the ASTM International F42 committee of standards has put SLM under the "laser sintering" category but this is an acknowledged misnomer since SLM completely fuses the metal powder into a true homogenous solid which is distinct from SLS as it is real sintering. Similarly, DMLS is another misnomer because of commercialization [13]. However, EBM (Electron Beam Melting) is truly similar which just replaces the high-power density laser with an electron beam for energy.

An assortment of combinations can be utilized by SLM to give us useful models made of the same material and functionality of production quality. As the segments are assembled layer by layer, it is conceivable to structure natural geometries with intricate internal features and difficult sections that cannot be cast or generally machined. And this package produces a final product that is long lasting for either prototype development or for the end user itself [14].

The idea is in the CAD model which the software slices into multiple layers of thicknesses between 20 and 100 μm so the image can be considered 2 dimensional for all practical intents and purposes. It is generally based on the *.stl* file (stereolithography) which again hints at the origin of this technique. The *.stl* file can be exported from any mainstream CAD program like SolidWorks and CATIA V5, which is then imported into a generally proprietary software of the manufacturer where values and parameters are assigned including physical supports to prevent extremely delicate and thin models from collapsing onto itself, which in all, helps the AM machine to literally 'print' the required model like a paper printer over 3 dimensions.

A slim layer of atomized fine metal powder is equally dispersed with the help of a coating mechanism onto a substrate plate, typically movable with computer control, vertically (Z) axis.

This happens inside a chamber containing a firmly controlled environment of gas, either argon or nitrogen at oxygen levels underneath 500 sections for each million. When each layer has been appropriated, each 2D cut segment of part geometry is melted selectively by laser over the powder. This is done with a powerful laser, more often than not a ytterbium fibre laser with several watts. The laser shaft is coordinated in the X and Y bearings with two high-frequency scanning mirrors. The laser vitality is exceptional enough to allow full liquefaction of the particles to shape a strong metal. The procedure is rehashed layer upon layer to completion. The recoating mechanism recoats the surface with more powder after each layer is fused.

2.1.3 Applications

Sometimes 3D Printing simply becomes infeasible even today on a cost basis when considered against more traditional techniques like casting, moulding and machining. There can also be some additional machining required for any metal manufactured through Additive Manufacturing (AM) due to some design constraints. There is also a lot of time and cost required to develop a special model with the manufacturer to ensure compatibility due to machine restrictions of the minimum resolution required, strengthening of such points in the design so it does not collapse and other such factors unique to AM can also come into play. But if the inherent lead times are longer with very small batch sizes and high costs, then additive

Figure 2.2 CFM International's 3D printed fuel nozzle which reduces part count from 18 to just 1[17].

is a much better fit there, such as is the case with the Aerospace industry. General Electric's now famous fuel nozzle is one such example on the Airbus A350 XWB aircraft [15]. Boeing even ordered some structural components printed with Titanium for the 787 Dreamliner [16].

Weight Reduction: Internal combustion engine's valves have been produced 'hollow' with over 20% weight savings in contrast with the Original Equipment Manufacturer (OEM) part without having any ill effect on failures, internal cracking and significant deformation [18].

Reverse engineering: Existing parts can be improved like an Air Inlet on a car for improved performance [19].

Ease of Manufacture: It is sometimes possible to not only reduce the weight (by 35%) but at the same time increase rigidity by 20% of a steering knuckle for a Formula Student car [20]. This was easy enough to be done by a group of students and help them finish first in Europe just because of AM alone, by lightening the load of critical steering components.

Professional Design: There is a strong drive in Formula 1 racing itself to see a reduction in component weights, even by mere grams as it can translate to faster lap-times, even by a millisecond. Nearly all teams use it including Red Bull. The DMLS improved geometry with Titanium64 material, for hydraulic components, thereby directly translating to over 250% better flow characteristics in the production of channels and bores, over the previously used techniques [21]. History has recorded Red Bull domination and won several consecutive constructor's championships. The Space Industry also extensively makes use of AM for rockets and satellites, like the Windform XT 2.0 currently in orbit amongst many others [22].

Sustainability: Adoption of AM also improves the sustainable aspects from an environmental point of view. Direct Digital Manufacturing revamps how we traditionally carry out operations with conventional manufacturing methods [23]. It can extend product life cycle, innovate environmentally friendly designs, improve logistics by reducing the need for transportation, reducing the need for inventory by not unnecessarily producing extra parts and help improve the product itself, integrally [24]. However, this is not a major driving point for most industries in general, especially those which deal with large volume productions [25]. It tends to find increased adoption only in small volume production, new product development and customization.

2.2 Dental Implants

The application of tribology with implications in biology is noteworthy in the investigation of lubrication effects, grinding and wear of oral delicate and hard tissues (like bones) with the advancement of helpful materials to differentiate genuine implants from counterfeit implants. The natural human tooth is already having phenomenal wear properties with a product lifetime coherent with the average lifespan if properly maintained by hygienically cleaning and regular scaling to remove calculus.

By understanding the impact of structural loading, the microstructure and frictional characteristics help us form relationships with those parameters than inhibit the product life of an implant. The oral cavity comprises of teeth, tongue, delicate tissues, and the temporomandibular joint (TMJ); which interfaces the jaw and palates on either side of the human face [26]. TMJ works as a synovial joint. Oral tribology is focused on the saliva, teeth and TMJ. In any case, harmful effects to the interface come into play because of rubbing and wear with respect to the jaw structure. The tooth structure comprises of an external enamel, inward dentine, pulp and dentine - enamel intersection (DEJ) [27]. DEJ exhibits fretting wear due to microstructural and mineral property variation of the enamel and dentine. The brittle enamel is also weak; where fragility is ascribed to the high modulus of Young's Modulus and tensile strength [28, 29]. Since the dentine is delicate and elastic, at the DEJ Junction stress gets dissipated across. For this capacity, this organic interface has high crack propagation. resistance upheld by strong dentine and various fundamental connective tissues to prevent cracking [30].

2.2.1 Impact of Lubrication by Saliva

Mastication, Thergosis and Bruxism, ordinary oral activities lead to slow but, eventual wear even in the best of oral health. High loads on contact and sliding may prompt loss of impeccable occlusal contact, tooth flexure, or ensuing tooth (enamel) loss [30]. The tooth enamel is exposed to the oral pit condition and occlusal forces. Wear and tooth misfortune results from whittling down, scraping or high shear stresses.at the cervical (neck) area surpassing shear stresses of the less versatile enamel [31]. Here, the capacity of salivation is critical by acting as a lubricating agent among delicate and hard oral tissues can also help in decreasing erosion and wear; tooth shape and position can limit saliva lubrication leading to increased wear at those places. Compelling tribological application is seen in vivo, by the arrangement of salivary film through layer-by-layer adsorption of protein on all strong substrata and mucosa layers

presented to the oral condition. Adherence of salivary film to tooth surface indeed depends on how effective it can lubricate the teeth, it falls under the Boundary Lubrication regime [32]. It was also discovered that the adherence of salivary film lessens erosion coefficient by a factor of 20 [33].

Be that as it may, in different test conditions, dental erosion may worsen by bacterial presence introduced from food forms and can result in accelerating tooth disintegration by the formation of plaque or calculus which will eventually get infected, needing extraction if not treated in time. Lessening the pH and making it acidic is what happens here and is known to influence tooth wear rate as the corrosive disintegrated enamel, is made progressively defenceless because of decline in mechanical properties from poor hygiene [34, 35].

By and large, a wonder of tribo-corrosion is seen by a consolidated impact of disintegration by demineralization and the scraped area of the same demineralized surface. Saliva enzymes are known for its ability to restore the enamel by dissemination of calcium, fluoride and phosphates particles from its rich film to the enamel [32]. For the same reason, Toothpaste is enriched and openly advertised by many companies for their calcium and fluoride content and helps restore or protect teeth by refurbishing the required minerals and elements.

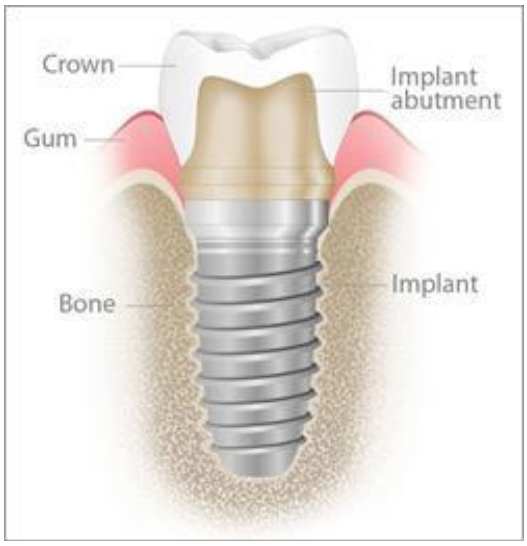

Figure 2.3 Example of a Dental Implant [36]

For those affected either by poor hygiene or accidents (car accidents and workplace incidents) and having to extract a tooth, they look for implants. And this is where the significant application of titanium is also seen in biological implants due to their high strength, low weight, corrosion resistance and biocompatibility.

2.2.2 Additive Manufacturing and Dental Implants

Additively produced titanium inserts empower mechanical properties that are financially infeasible with conventional subtractive methods [36]. Unique and specific to the patient, biomedical implants can be produced that comply with explicit surgical geometries by impersonating the mechanical properties of common bone, and assist in better cell and tissue integration, through the use of custom-made microtextures which are fine-tuned and tailored to fulfil prerequisites for cellular interaction and cellular proliferation.

Regardless of the opening of doors in the field for medicinal advancement empowered by titanium AM, a progression towards the need for difficult specialization must be controlled to help in the daily schedule of dental doctors. The deployment of tools for such control must be financially attractive. A vital condition for the commercialization of AM in a clinical setting is that these specialized necessities be computerized inside master frameworks and related plan for AM (DFAM) instruments whereby explicit embed geometries are algorithmically characterized. DFAM instruments are particularly important for the plan of AM cross section structures because of their high intricacy [37].

A required part could be taken to show a rundown of the specialized structure difficulties that exist for the manufacture of AM titanium inserts. Contingencies for limiting a structure's multifaceted nature are to be identified, and so are the dynamic research difficulties. This work for the part would additionally fill in as a source of perspective for the improvement of novel research commitments and DFAM devices by recognizing those contingencies that are either rising or stay as controversial or open-for-research questions.

We can be hinted at the Just in time (JIT) culture of other industries like automotive manufacturing whereby DFAM instruments are incorporated with robotics and imaging technologies to produce those implants that are specific and unique to patients within the surgical environment, as and when required by the dental surgeon. The implants can be produced 'on-demand' and quickly to save costs in logistics, inventory and production. Especially, if those implants need to be customized, they fall into low and medium volume production which is theoretically feasible for AM manufacturing processes.

2.2.3 Bone Tissue Engineering (Osseointegration)

Bone is naturally, a composite material which is approximately constituted of the following constituents and chemical composition [38]:

1. 10-20% of water,
2. 20-30% of the matrix,
3. 45-60% of minerals.

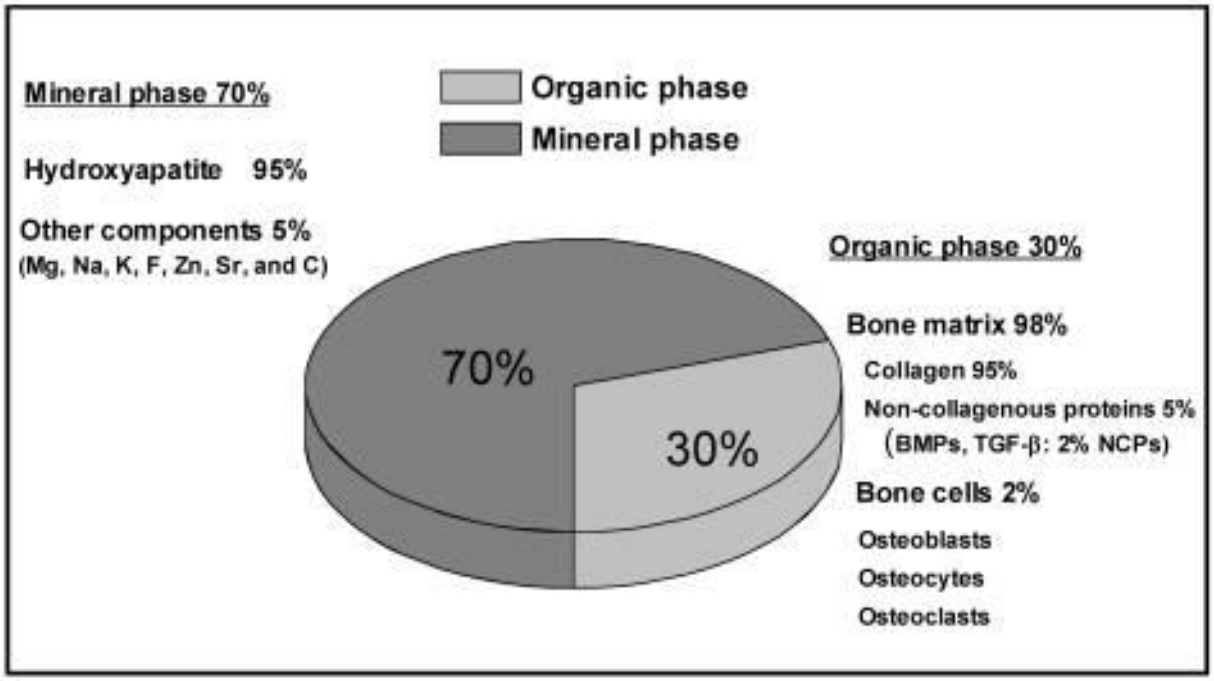

Figure 2.4 Bone's chemical composition, water is included under the Organic phase [38]

Osteoblasts are cells that secrete the ‘bone substance’ which forms the bone from a matrix, after mineralization, naturally. Their proliferation is essential to ‘integrate’ and embed the implant into the body. The jaws are no exception and are basically bones.

It has always been a troublesome issue to treat bone imperfections and defects. Bone grafts are required for imperfections bigger than their cross-sectional diameter by 1.6 times [39]. The graft can be of two types from a medical perspective, autologous graft (taken from another bone in the same body) and allograft (taken from a cadaver, a dead body). However, both grafting sources have restrictions with the risk they impose of infection, rejection by the immune system and pain (from the donor site, in case of autograft) [40].

Titanium alloys have been extensively used in orthopaedic surgeries and dentistry because of safety and mechanical properties. This also eliminated the need to look for donor sites or cadavers as they may not always be desirable. By 3D Printing, we can allow for and control, porous connected structures with high-precision and patient-specific personalization. This forms a good substitute for bone defects for clinical needs.

Scaffolds

Through scaffolds, we can help minimize the amount of Titanium we use since it is known to be bio-inert and incapable of bone cell proliferation [41]. Multitudes of researchers have experimented with scaffolds of various parameters of strut size, pore size and porosity on both animals and humans.

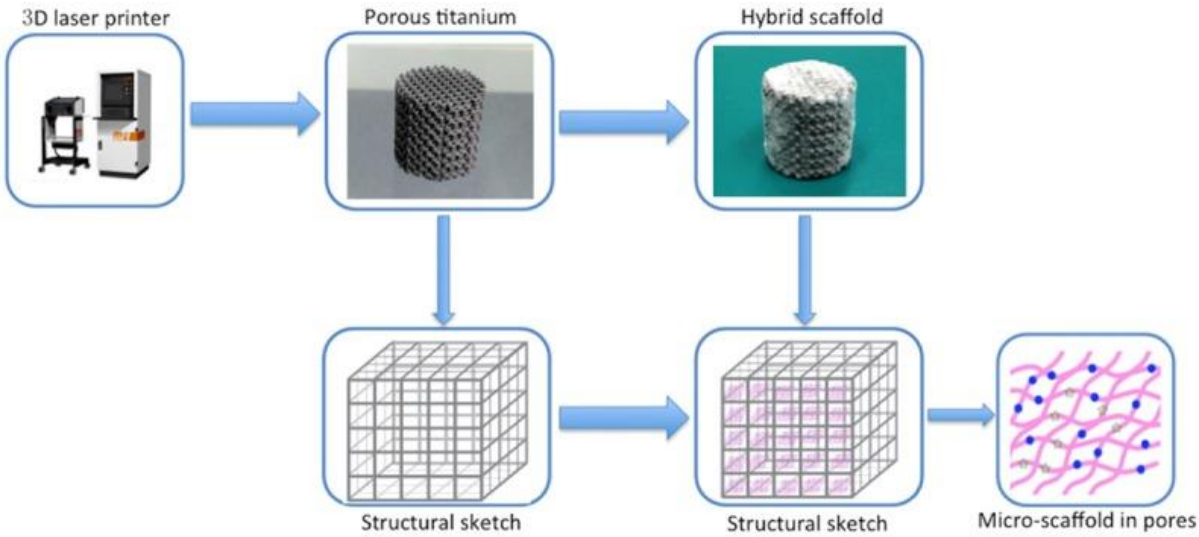

Figure 2.5 Additively Manufactured Titanium Scaffold schematic, modified by Gelatin within the pores for improving Osteogenesis [42].

Titanium alloys have been used since a long time (especially the Grade 5) for biomedical implants and the 3D printing methods have permitted these alloys, to be utilized as an implant, designed exclusively, with high porosity and a versatile modulus fitting for clinical needs. Scaffold Porosity can reach > 80% with enormous pores, which not just gives adequate space for bones to grow while ensuring superior nutrient and supplement transport [43] yet in addition also helps ease protect bone from stress during the time spent during bone development [44]. Along these lines, > 80% space can meet clinical necessities. Also imparted to the implant is a strong resistance to absorption which then helps give a solid mechanical advantage, evading the danger of confusion by the immune system between purported degradation of implant material and new bone development, which can prompt genuine results, confirmed even from testing on the calvarial bone of rabbits [45].

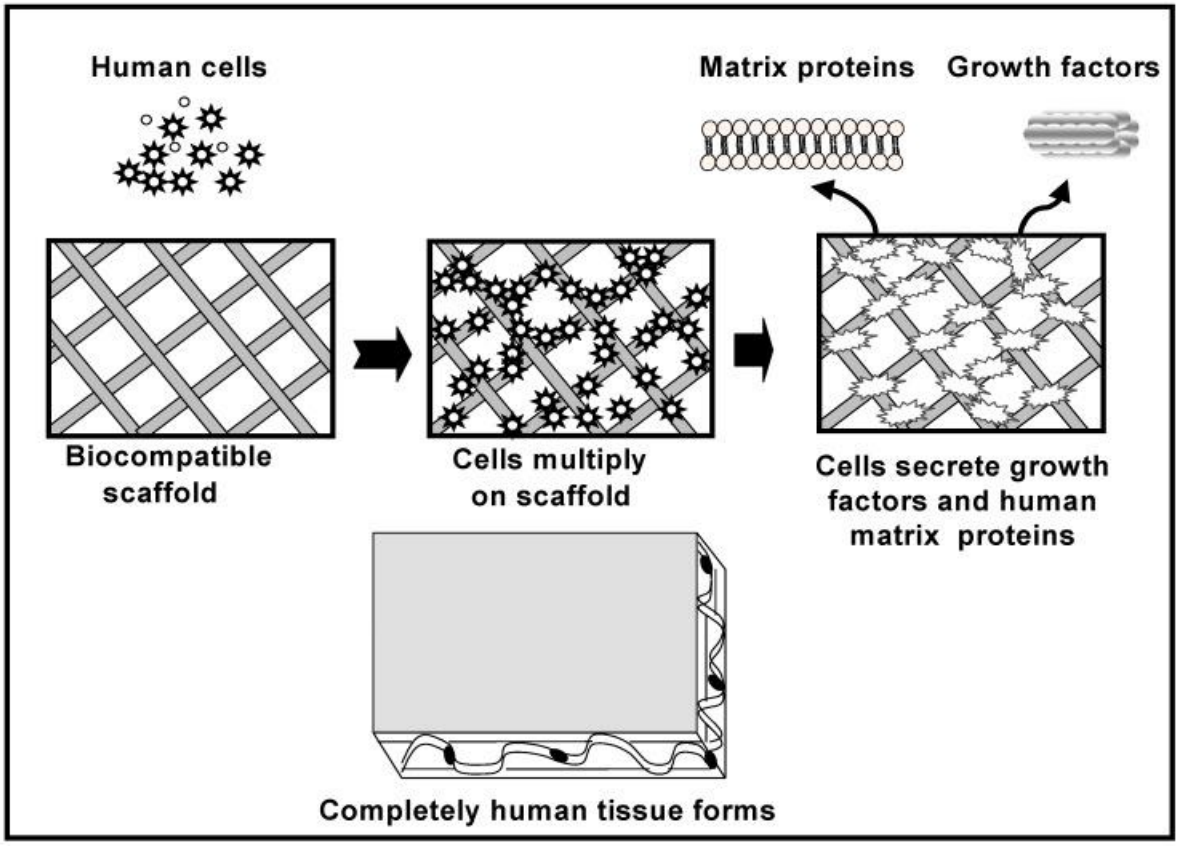

Figure 2.6 Schematic for a Cell-based bone cell regeneration from a Titanium Alloy scaffold [42]

We already know that Titanium alloys make a great choice for orthopaedic applications because of their high strength to weight ratio, biocompatibility and other mechanical properties. Because of the advents in AM, we can now make lattice structures which impersonate the mechanical properties of the bone. By synthesizing a three-dimensional micro-scaffold structure, we create an effective method to modify and tailor porous titanium which sustains conditions suitable for cell proliferation whilst additionally being used as a carrier of bioactive factors in the future.

Fatigue

Many researchers have already discussed the fatigue behaviour of porous titanium Grade 5 like Ti-6Al-4V scaffolds by Selective Laser Melting [46], cellular Ti-6Al-4V produced by Electron Beam Melting [47], titanium Grade 5 Mesh Arrays produced by EBM [48], produced by Magnesium Space holder technique, a powder metallurgical process [49] and pure titanium with 50-70% porosity [50]. The result of these studies concludes that the fatigue performance of the Ti lattice structure is eerily similar to porous aluminum.

Titanium Grade 5's scaffolds endurance limit is about 0.1–0.25 of their yield strength. The bulk Ti-6Al-4V material produced using traditional methods has an endurance limit of 0.4 of

the yield strength [47]. The discrepancy here for the same Ti-6Al-4V can be as a result of the notch sensitivity, the unpolished surface of struts, significant porosity in struts, residual stress, and microstructure [48].

A Lattice structure cannot undergo mechanical treatments like shot peening to increase fatigue strength or heat treatment could be used instead [51]. Some researchers have also shown that hot isostatic pressing treatment will dramatically improve the fatigue life of Titanium Grade 5 scaffolds [52]. Furthermore, another study explored the three kinds of meshes (rhombic dodecahedron, G7 and Cubic) of Titanium Grade 5 alloys to show the link between cell morphology and it is compressive fatigue behaviour [53]. The fatigue mechanism that they uncovered for these 3 types of meshes as the interaction of propagation of strut fatigue crack from bucketing, cyclic ratcheting and strut bending deformation.

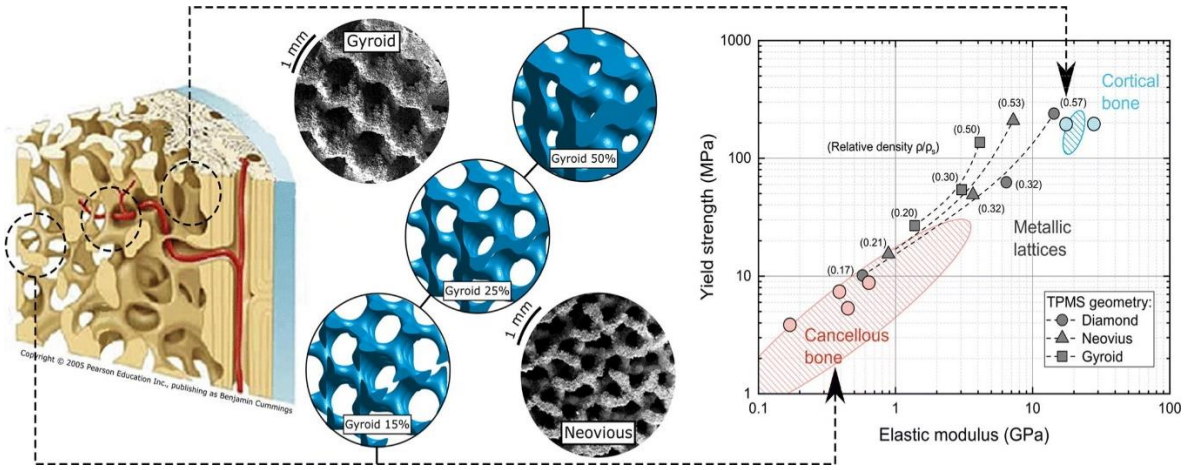

Figure 2.7 An example of tailor designing with SLM for Different Triply Periodic minimal surfaces of Ti-6Al-4V helps to suit the type of bone, since not all bones are created equal, demonstrating the dependence on Geometry and Density [54]

In conclusion, to successfully design a biological organ (i.e. Bone) that encourages natural tissue proliferation, three basic phases are required as follows [38]:

- Osteoblasts and Osteocytes (osteogenic cells) and/or signalling biomolecules
- Quantitative measures of Bone tissue's regenerative outcome, and
- Biocompatible scaffolds like Ti-6Al-4V that is instrumental for normal bone cell functions.

2.2.4 Tribology and Dental Implants

It was found on a patient that before an implant, their masticatory force (maximum biting force) ranged at 4.5-25.3N, followed by 10.2-57.5N, 3 months post-treatment [55]. In Literature, movements are not reported to be linear, in one direction.

Studies have shown that occlusal surfaces undergo an oscillatory tangential displacement of small magnitude as fretting or reciprocating sliding with major displacements over time. Counteracting frictional forces are generated and innate to the reciprocating sliding motion. Contact forces, displacement amplitude and surface materials themselves, have an important effect on the friction forces which depends on the coefficient of friction of the oral system. An experiment of stainless-steel bracket-wire combination under small oscillating displacements

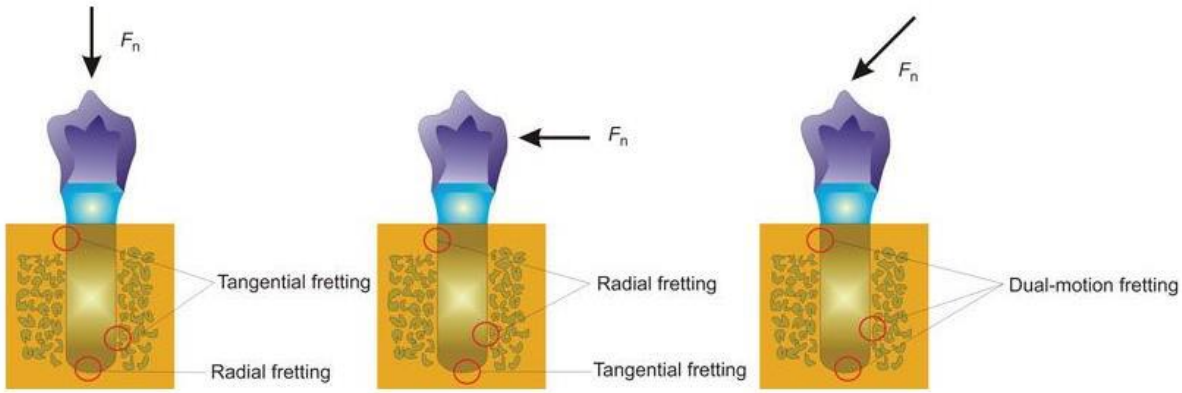

Figure 2.8 Reactive forces on a dental implant from normal functioning [58]

by Willems et al showed a significant increase in friction coefficient values (0.45-0.97) due to the combined effect of static and dynamic friction [56]. Higher friction values were linked to the offset from the centre positioning of the orthodontic wire. Higher friction due to prolong micromovements triggers wear. In literature, the most common cause of material loss in a dental implant is Abrasive wear (scratching). Jalbrzykowsk et. al attributed 40% of all implant damage to abrasive wear, similar for screw fracture and 10% accounted for chemical degradation [57]. Excessive wear generates debris, delamination (third body effect), adhesive (galling and scuffing) wear, rolling contact fatigue and Tribocorrosion depending on the environment.

Chapter 3

Methodology

The experiment consists of 4 parts.

1. Sample Preparation: One sample was prepared with a specimen produced by Selective Laser Melting (SLM) process and the other sample was produced using traditional/conventional manufacturing process, both classified as Ti6Al4V (ASTM Titanium alloy Grade 5). Measurement of some roughness parameters can be performed, for both samples at this stage, using a profilometer after polishing.
2. Electrochemical Experiment: Linear Polarization Resistance (A variant of standard ASTM-G59-97) was performed for both samples. This enables the measurement of the corroding system's polarization resistance.
3. Tribological Test: Reciprocating sliding configuration was used with different loads for each sample sliding against a Zirconia ball as a counter body with a ball-on-flat setup.
4. Evaluation: Each wear track on the specimen was evaluated using an infrared Laser Profilometer in order to calculate the Ti6Al4V wear volume with 200 number of scans over the length of 3 mm and a resolution of 1000 points over a width of 4 mm at a scan rate of 500 μm/s. Each wear scar on the zirconia ball was observed with an optical microscope in order to calculate the Zirconia ball wear volume. Microstructure analysis can be performed in the future for better understanding of samples at hand.

3.1 Sample Preparation

Two specimens of Titanium Grade 5 (Ti6Al4V) were prepared. One produced by the traditional/conventional method. The second sample was obtained from SLM method with the composition and mechanical properties shown in Table 3.1 and Table 3.2, respectively.

Note: “Conventional” will be used to refer to the sample produced using conventional/traditionall subtractive methods and “SLM” will be used to refer to the sample produced via Selective Laser Melting; unless specified otherwise. The decimal separator used in the entire document is a dot.

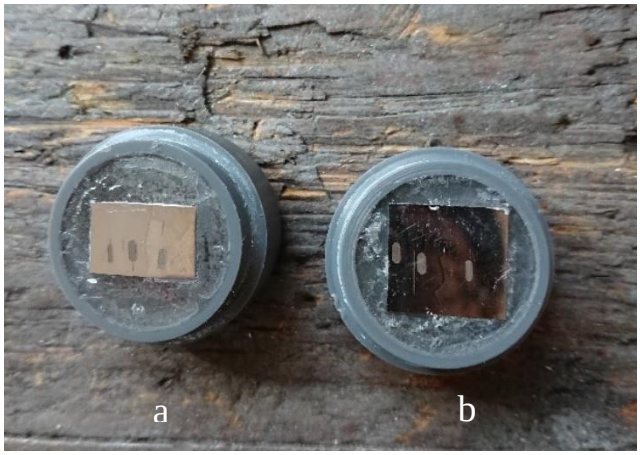

Figure 3.1 Ti6Al4V samples: (a) produced by conventional method and, (b) produced by SLM.

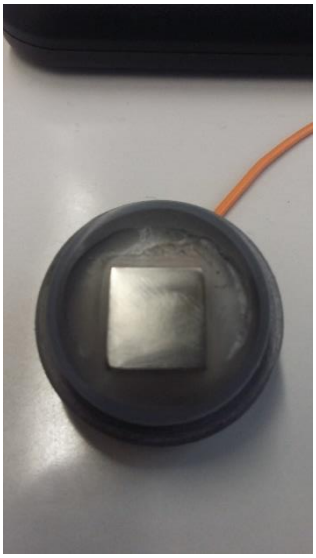

(a)

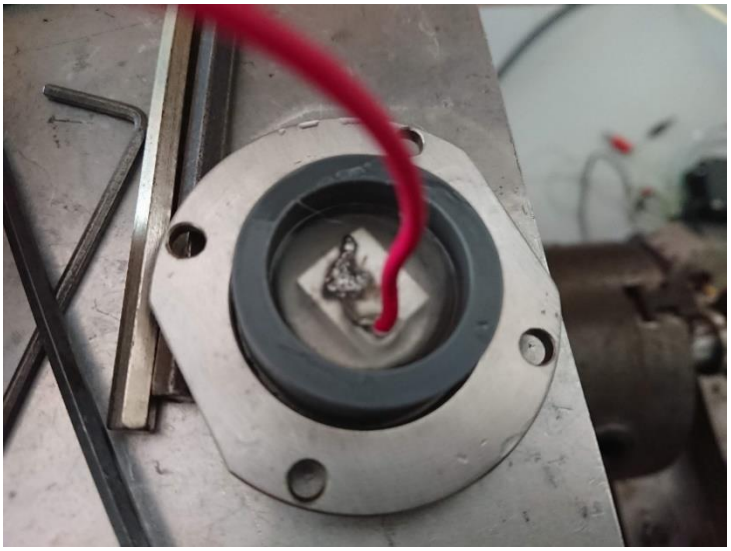

(b)

Figure 3.2 (a) top view and; (b) underside of the Ti6Al4V sample to which a wire was soldered.

Table 3.1 Chemical composition of titanium alloy Ti6Al4V produced by SLM [59].

Chemical Element	**Al**	**V**	**Fe**	**C**	**O**	**N**	**H**	**Ti**
Weight (%)	6.2	4.1	0.17	0.06	0.14	0.03	0.009	Remainder

Table 3.2 Mechanical Properties of the Ti6Al4V sample produced by SLM [59].

Hardness [HV1]	**Young's Modulus [GPa]**	**Yield Strength [MPa]**	**Tensile Strength [MPa]**
358	120	1147	1000

The specimens were cut with a grinder, an abrasive cutting process to a suitable size, as to fit in the plastic casing as seen in Figure 3.1 before polishing. After polishing, an insulated wire was stripped free of insulation at both ends (to establish a better contact), with one end being soldered to our cut samples. A closed circuit was established by testing it with a multimeter.

Then the cold-cure epoxy resin mixture was created with a suitable amount of filler powder to hold the samples securely in their plastic casings while simultaneously shielding the soldered wire from the environment. It was then left overnight for the curing process to complete with the polished surface remaining exposed to the ambient air.

Both of the samples were subject to abrasive grinding with SiC sandpapers of grit 300, 800 and 2000 respectively. The progress to the next sandpaper was made when all the scratches from the previous grit were gone and a shiny mirror-like finish was obtained at the end. A colloidal Silica suspension was also used for final polishing. After this, they were cleaned with acetone and distilled water, then left to dry.

Using the *Mitutoyo Surfest – 500* profilometer, roughness measurements can be taken to measure the parameter like R_a, R_q and R_z. These measurements are in accordance with ISO standard 4287.

The composition of the artificial saliva used as lubricant/electrolyte is listed in Table 3.3 [60]. The exposed surface area of the sample was calculated and is also listed in Table 3.4.

Table 3.3 The Chemical Composition of the Artificial Saliva used in the experiments (g/L).

NaCl	KCl	KSCN	$NaHCO_3$	KH_2PO_4	$CaCl_2.2H_2O$	$Na_2HPO_2.12H_2O$	Citric Acid	pH
0.6000	0.720	0.060	1.500	0.680	0.220	0.856	0.030	6.5

Table 3.4 Reciprocating Ball on Flat configuration for the tribological experiment.

Specimens (Flat)	Counter body (Ball)	Fluid Medium
Ti6Al4V (SLM) Surface Area: 2.34 cm^2	Zirconia (ZrO_2)	Artificial Saliva
Ti6Al4V (Conventional) Surface Area: 1.54 cm^2		

3.2 Electrochemical Evaluation

All experiments were carried out with the previously described device consisting of a tribometer made from a retrofitted lathe machine with an integrated conventional three-electrode cell set up.

The three-electrode cell was composed by a Saturated Calomel Electrode (SCE) that works as reference electrode with a constant potential (242.2 mV vs. SHE - Standard Hydrogen Electrode) which is the model Radiometer XR110 reference electrode. It consists of a glass body, saturated calomel reference system, refillable electrolyte (sat. KCl), ground joint, and porous pin junction as described by the manufacturer *Hach*. This was coupled with a platinum sheet counter electrode, model XM120. It is recommended for Voltammetry applications like our experiment.

A schematic setup is represented in Figure 3.3. It is exaggerated and simplified, for ease of understanding. The polycarbonate container holds the sample inside, keeping it submerged in the electrolyte (artificial saliva). An O-Ring rubber seal at the bottom ensures the bottom of the sample remains dry and the hole beneath makes it possible for the wire to exit the container.

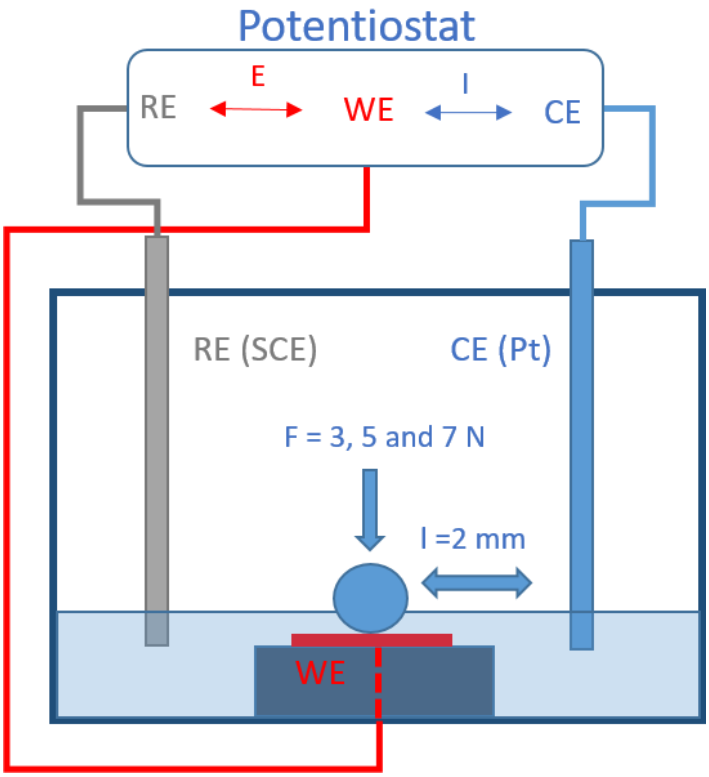

Figure 3.3 Schematic model of the setup with WE: Working Electrode, RE: Reference Electrode and CE: Counter Electrode connected to a Potentiostat with a Zirconia ball held under a Normal Load from a spring, adjustable by tightening or loosening a bolt (not shown) as appropriate to modify the compression load on spring.

The SCE with the help of an external cable from the screw cap to the Potentiostat (Bio-Logic science instrument SP-50) which is connected to a computer A. It was controlled by EC lab version 11.26 (December 11, 2018). The firmware on the Potentiostat was also updated to ensure the best possible performance upon the strong recommendation of the sales engineer

from Bio-Logic Science Instruments ESPAÑA, S.L.U as this is the last version that will be developed by the manufacturer.

Figure 3.4 shows the input parameters at the EC-lab software in order to perform a Potentiodynamic Polarization curve using the linear polarization resistance method.

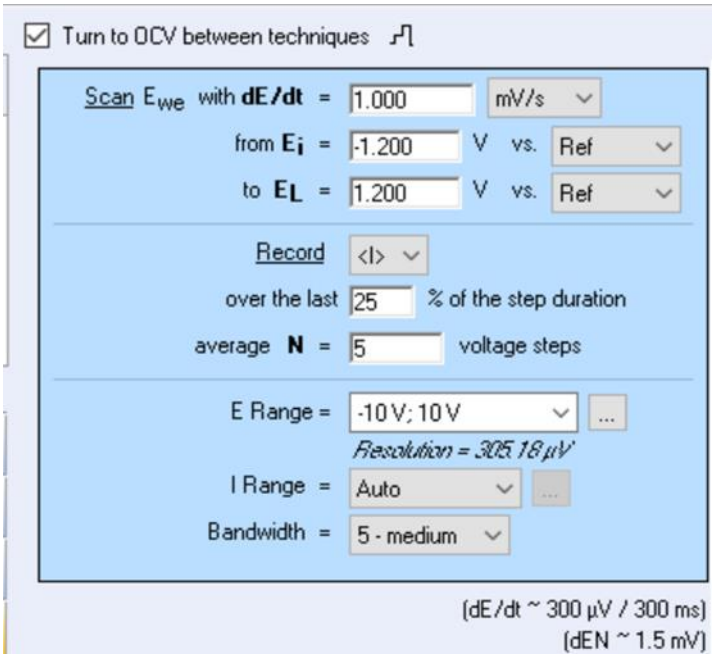

Figure 3.4 Example of input parameters for performing Linear Polarization Resistance method.

3.3 Tribometer

The Tribometer is used in conjunction with the electrochemical equipment. The ball-on-flat configuration establishes a reciprocating sliding motion, where flat surfaces represented all test samples. The rubbing counterpart was a zirconia (ZrO_2) ball with 10 mm diameter.

The Tribometer used is an ingeniously retrofitted lathe machine with load cells (for tangential and normal loads), polycarbonate container for the sample and a beam to hold the sample in place while mounted to a bearing which translated the rotational motion of the lathe machine to a reciprocating one. The lathe was calibrated to rotate at 180 rpm to give us a 3 Hz frequency for testing with a fixed electrical controller.

The reciprocating sliding tests were performed with a load of 3, 5 and 7 N on each of the two samples. The frequency was not varied and was fixed at 3 Hz for each run corresponding

to 0.012 m/s of average linear velocity. The sliding time was set to 1250 seconds on LabView software to give us 15 m of sliding distance for both samples (Conventional and SLM).

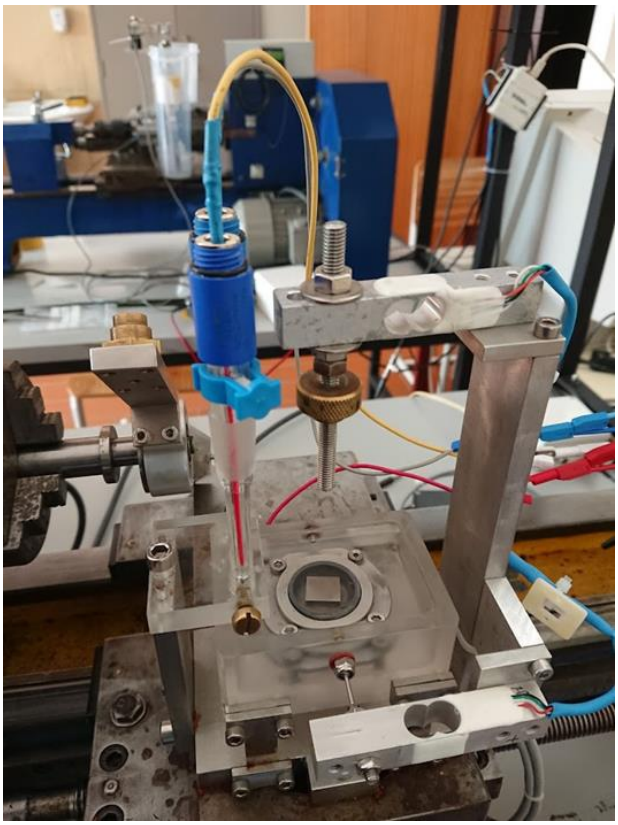

Figure 3.5 Experimental Setup of the Triboelectrochemical cell.

During the setup, the samples (each per test) were set on the stage and immersed with the artificial saliva. The artificial saliva was replaced after every single run. Contact was then made between the ZrO_2 ball and sample (working electrode) before the load was applied and rubbing was initiated. Open Circuit Potential measurements were taken for 1 hour after setting up the experiment. The sliding distance was set to 15 m with the frequency of 3 Hz, a rubbing time of 1250 seconds for the run. After sliding, the potential was monitored for 1 hour to record it reach equilibrium again. Figure 3.1 shows the images of the test samples after triboelectrochemical experiments. The sequential test procedures are summarized in table 3.5.

Chapter 4

Results and Discussion

This chapter will present with the outcomes of Chapter 3 – Experiments methodology and analysis of these results.

4.1 Electrochemical Behavior

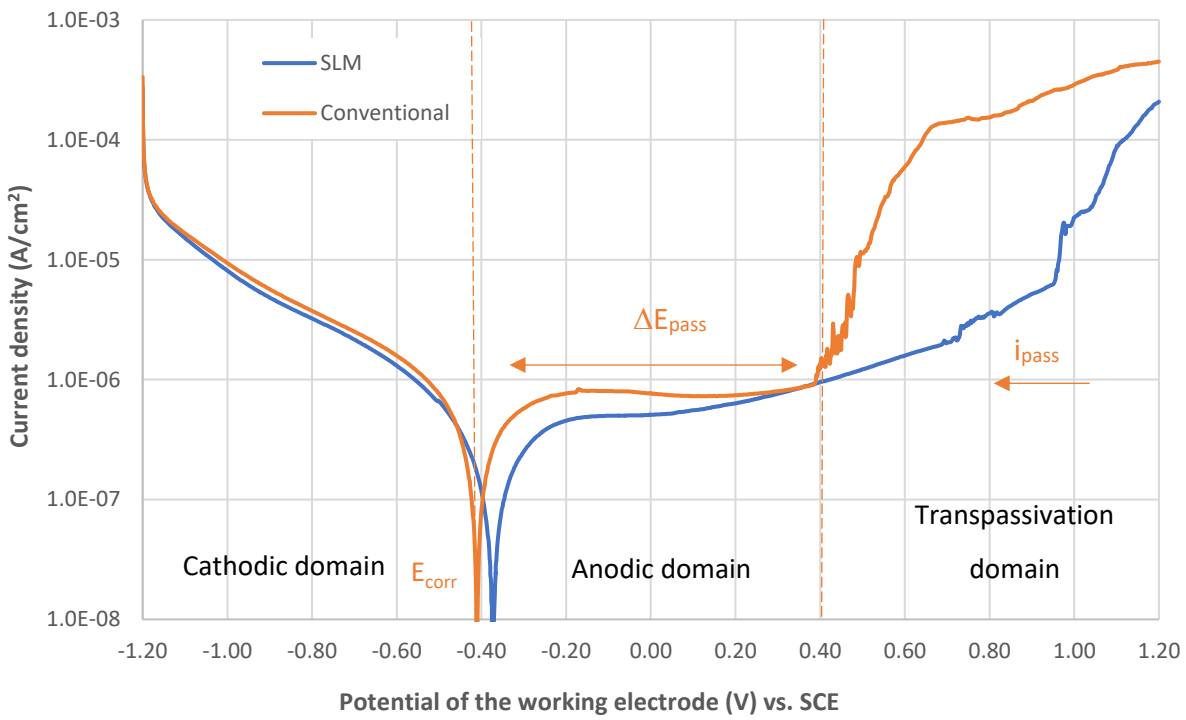

Figure 4.1 Potentiodynamic Polarization curves for Ti6Al4V alloy produced conventionally (orange curve) and by SLM process (blue curve). The different domains and different corrosion parameters are exemplify for the Ti6Al4V obtained by conventional process (orange).

It can be seen at Figure 4.1, by analyzing the potentiodynamic polarization curves for both Ti6Al4V samples that the passivation occurs, when immersed in the artificial saliva, at potentials between approximately -0.3 and 0.6 V vs. SCE. At this potential range, the current (i_{pass}) remained approximately constant with increasing potential due to the formation of a stable protective passive film composed of a very thin oxide layer of TiO_2. However, the

conventional sample has both the cathodic and anodic branches slightly shifted to the highest current densities when compared to the SLM sample.

The latter clearly has much flatter (horizontal) curve. At high anodic potentials, extremely high current density was recorded due to the dissolution of the TiO_2 protective film probably from the attack of chloride ions in the electrolyte enhancing corrosion. Furthermore, there can be increasing dissolution of metals once the 'protective' oxide layer has worn off.

We can thus conclude by observation of Figure 4.1 that the SLM specimen does not lose its protective oxide layer as fast as the conventional specimen since the transpassivation domain starts at higher potential values (> 0.7 V vs. SCE), while for the conventional sample the transpassivation domain started at approximately 0.40 V vs. SCE.

Corrosion preferential sites in the alloy's α and β phases, as well as α′ martensite, have been identified by researchers [61]. The β phase is more stable and imparts better corrosion resistance. They also identified an increase of corrosion resistance in Electron-Beam Melting (EBM) produced Titanium Grade 5 from 0.0128 to 0.0037 mm/year when the scan rate was changed from 0.166 to 0.05 mV/s. when in artificial corporal fluid (Hank's Solution) to credit the formation of TiO_2 passive layer. The passive layer gets formed and maintained better.

An investigation into SLM produced Titanium Grade 5 showed most corrosion resistance in the direction of the build (upwards), showing that this property can be anisotropic [62]. They showed significant corrosion resistance in the XY direction as compared to other planes. Their sample had each layer oriented at 90º to each other. They also reported more pits in the XZ plane indicating that the passive film over it is not resistive enough. Due to the higher cooling rate and thermal gradient during the production of SLM Ti6Al4V alloy, there is a higher occurrence of acicular α′ martensite and less β-Ti phase which imparts inferior corrosion resistance to XZ plane [63].

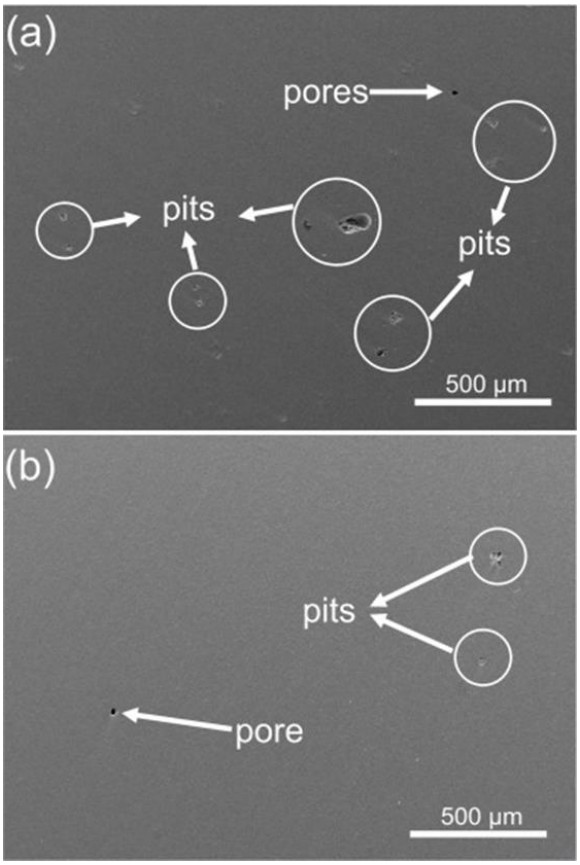

Figure 4.2 More pits seen in (a) XZ plane than (b) XY plane on SLM produced Ti-6Al-4V [62].

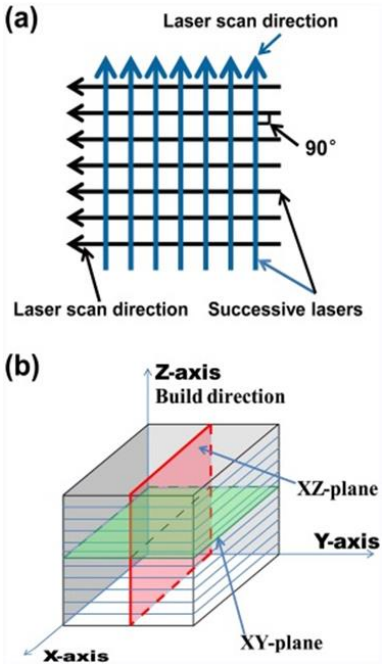

Figure 4.3 Schematic of (a) Laser scan direction and (b) 3D diagram of SLM produced Titanium Grade 5 [62]

Analogously, this appears to be a similar case to the design of composites like Boron/Epoxy given constant properties for axial and transverse modulus, Poisson's ratio, shear modulus etc., can lead to very different properties for a same problem statement with the assumption that all layer thicknesses are same and temperature constant consequently gives us drastically different optimum thickness (weight) when the laminate orientation is the only parameter being modified. Optionally, it was solved previously with the Tsai-Wu failure criterion approximation here[2] in a separate document using MATLAB which can demonstrate the effect of laminae orientation after isolating everything else.

It appears that, perhaps, a similar case can be made for the SLM specimen and there is further scope to explore this hypothesis further by modifying the laser scan orientation and other scan strategies of the AM machine [62].

Table 4.1 Calculations of Corrosion Current, Corrosion Potential, ΔE and Corrosion Rate from the Potentiodynamic Polarization Curves

Specimen	E_{corr} (V vs SCE)	i_{pass} (μA/cm^2)	ΔE (V vs SCE)	Corrosion rate (mmpy)
SLM	-0.37	0.46	-0.25 to +0.72	1.86E-3
Conventional	-0.40	0.74	-0.29 to + 0.38	3.37E-3

4.2 Effect of applied load on OCP measurements

Figure 4.4 records the potential of the working electrode (E_{WE}) as a function of the sliding time during the rubbing experiment as well as an hour before and after it. Before the sliding test begins, the samples were immersed in artificial saliva for 1 hour to monitor the open circuit potential (OCP). During this time, the changes in OCP's slope of test materials were negligible. This suggests corrosion was minimal an oxide layer was in existence to retard metal dissolution since the samples were exposed to the artificial saliva solution. Once the samples were put under normal applied loads, and reciprocating sliding motion starts, a sharp drop in E_{WE}

[2] Internet required for hyperlink to OneDrive.

indicates how fast the passive oxide layer of the test samples was physically removed with each run of a different load. This is a mixed response of the system to mechanical and chemical action as each time we remove the oxide layer, it tries to reform again, so on and so forth. When the applied load and the reciprocating sliding movement ends, the surface of the sample it passivates again as it is possible to observe at Figures 4.4 and 4.5 by the logarithmic shape curve.

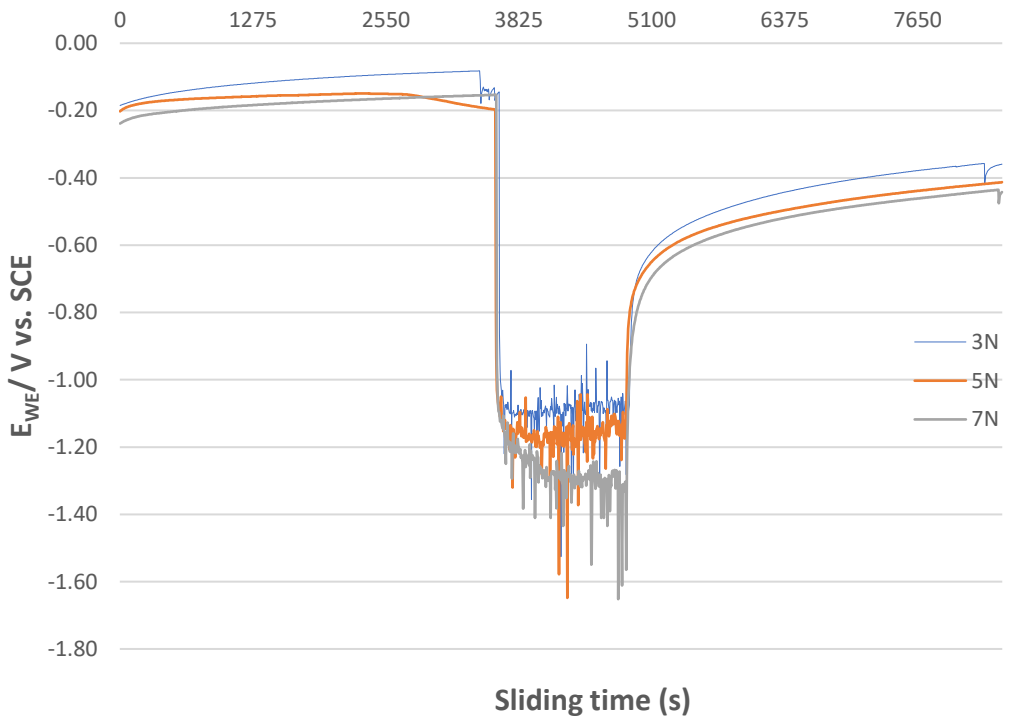

Figure 4.4 Evolution in the OCP of the Conventional sample with time - before, during and after reciprocating sliding test for each of the loads of: 3 N, 5 N and 7 N.

Load appears to play a slight role in passivation for the conventional sample as it takes longer time to reach the same level of free corrosion potential. Thus, there is some sensitivity to the applied load, even if it is small. In comparison to Figure 4.5, there is more sensitivity to different applied loads for the conventional produce sample than for the SLM sample.

It could be possible that the layering process has increased a net surface area of the SLM sample which exposes it to ambient oxygen better and faster and the increasing of the load to 7 N did not seem enough to bottleneck passivation sufficiently enough to see distinction like

shown at Figure 4.4. In other words, it could be possible for the submerged SLM sample to recover faster as more oxygen molecules from the environment could interact with it.

Furthermore, Ti6Al4V SLMed parts have been reported to be inherently rougher, with a typical roughness average (R_a) of 10 to 25 microns [64]. The wire fed AM machine produces parts with the most roughness and regardless of the source, any such part would need to be polished or machined to achieve levels of R_a between 0.1 to 0.4 [64].

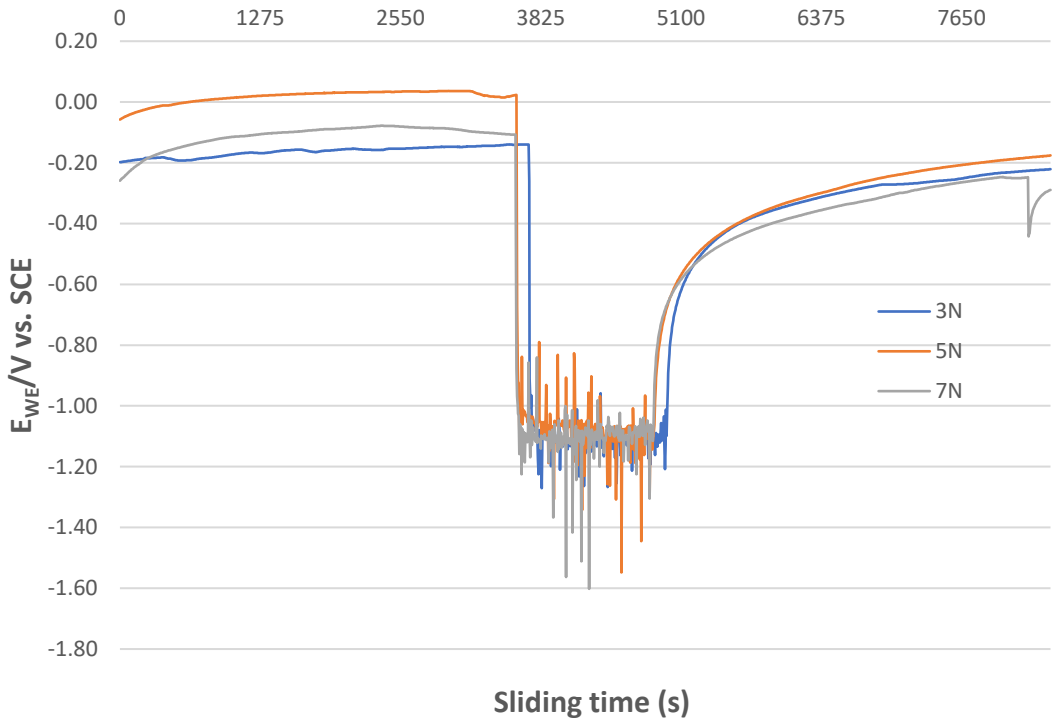

Figure 4.5 Evolution in The OCP of the SLM sample with time - before, during and after reciprocating sliding test for each of the loads of: 3 N, 5 N and 7 N.

Similar behaviour has been recorded for a cathodic shift at the onset of sliding by several researchers, Figure 4.5 also follows the same pattern [65, 66]. The magnitude of E_{WE} drop in the cathodic direction is presumed to be predominantly governed by gross slip mechanism and the strength of the passive film. However, the film potential fluctuations were observed to be more stable compared to other samples. The extent of the cathodic shift in both figures further confirms the onset of wear, removal of the passive protective oxide layer and increase in corrosion susceptibility of Ti6Al4V alloy in artificial saliva. Free corrosion potential or OCP

fluctuates in both Titanium Grade 5 alloy samples. As discussed before, this is happening because of periodic growth (re-passivation and) removal (de-passivation) of the passive film in the wear zone. Figure 4.6 symbolizes the periodic surface damage (the breakdown of protective oxide) in contact with a diagram.

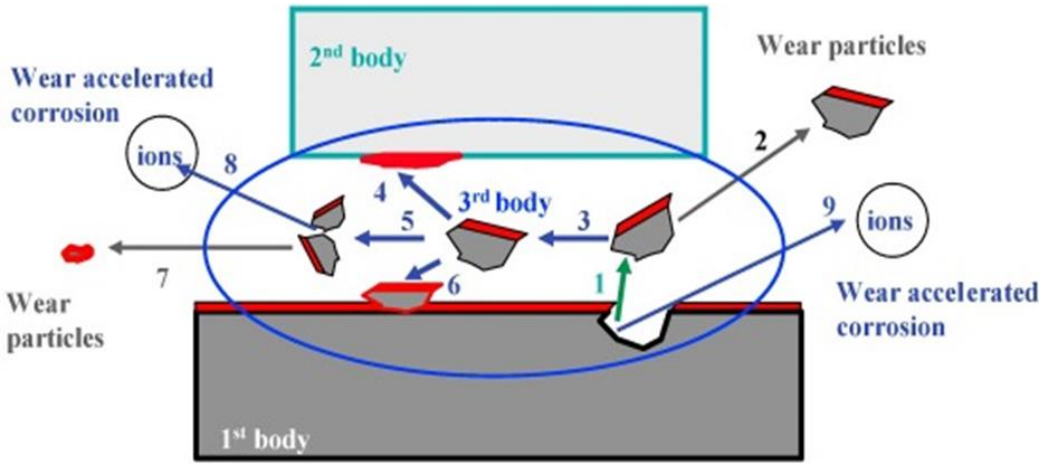

Figure 4.6 A schematic picture of the mass flow of the tribocorrosion system [67]

The fluctuations that we see in the rapidly changing directions can be directly interpreted as proportional to shifts of anodic: cathodic free corrosion potential. This stems from the presence of passive and active galvanic couples [67]. When the sliding is stopped, the free corrosion potential shifts in the anodic direction as film re-passivates on the worn area. Restoration depends on the extent of wear and the corrosion behaviour of the alloy as a galvanic couple is formed between the unworn (cathodic) and worn (cathodic) surface.

Between Figure 4.4 and Figure 4.5, we can see that the effect of loads on SLM is less when compared to conventional sample where the 7 N normal load has shown greater de-passivation during wear. Nevertheless, the difference remains small since the overall patterns show 7 N and 5 N cause more fretting than 3 N as can be thought along the lines of Hertzian contact pressures.

4.3 Friction behaviour

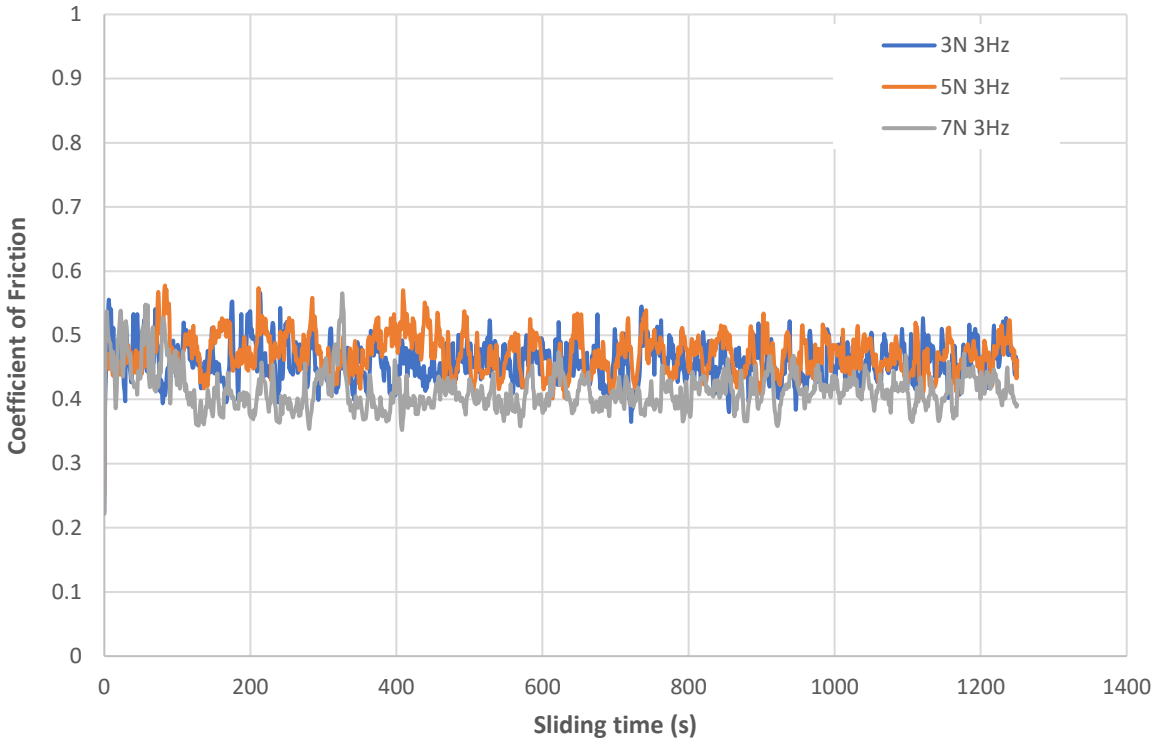

(a)

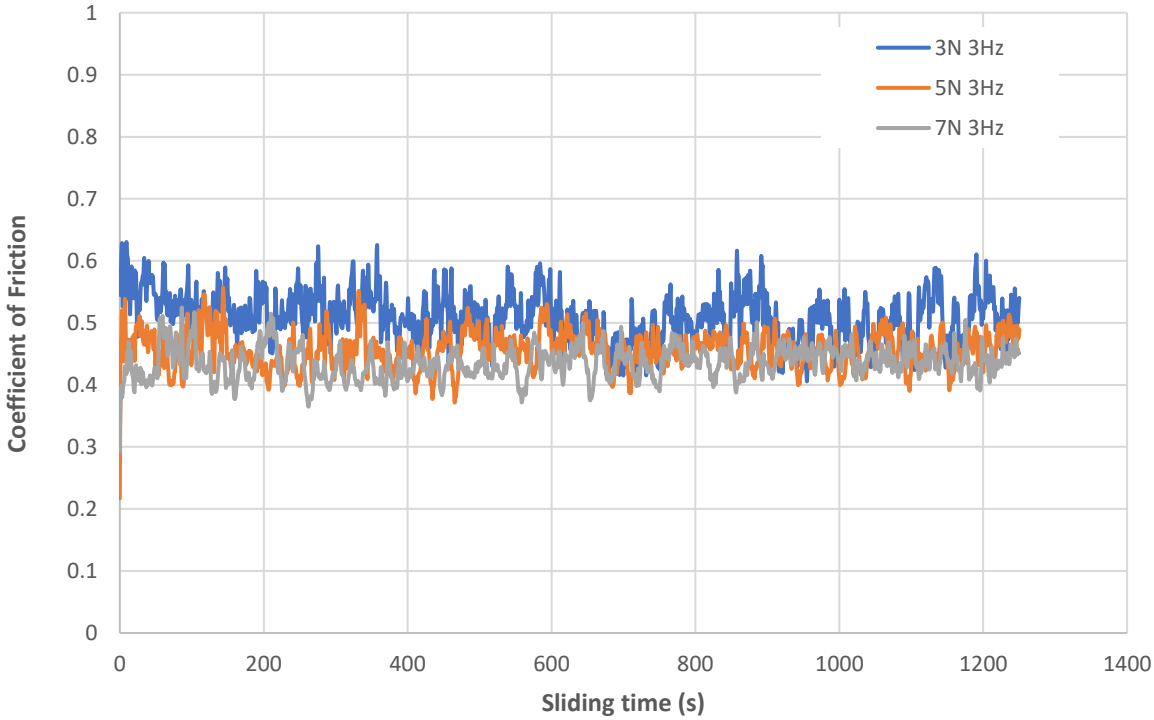

(b)

Figure 4.7 Evolution of the COF with sliding time for: (a) Conventional sample and; (b) SLM sample.

Figure 4.7 (a) and (b) show the evolution of the COF vs sliding time for the rubbing tests for both Ti6Al4V samples for different varying loads (3, 5 and 7 N), submerged in artificial saliva. It was recorded simultaneously with E_{WE} using the OCP technique discussed before albeit using a different computer with LabView connected to a pair of load cells which measured Normal Forces and Tangential Forces to give us the coefficient of friction. The normal force was controlled with the help of a clamped spring that can be tightened or loosened to achieve the desired value of normal force. The load cells were already calibrated prior to the experiments.

The 3Hz frequency was fixed by an electrical input to the lathe motor and confirmed with the help of a dual mode - digital non-laser photo tachometer as well as the contact type tachometer to achieve consistent rpm readings.

The overall mean coefficient of friction and standard deviations, for both samples can be seen in Table 4.2 and a column chart for comparison can be seen below at Fig. 4.8.

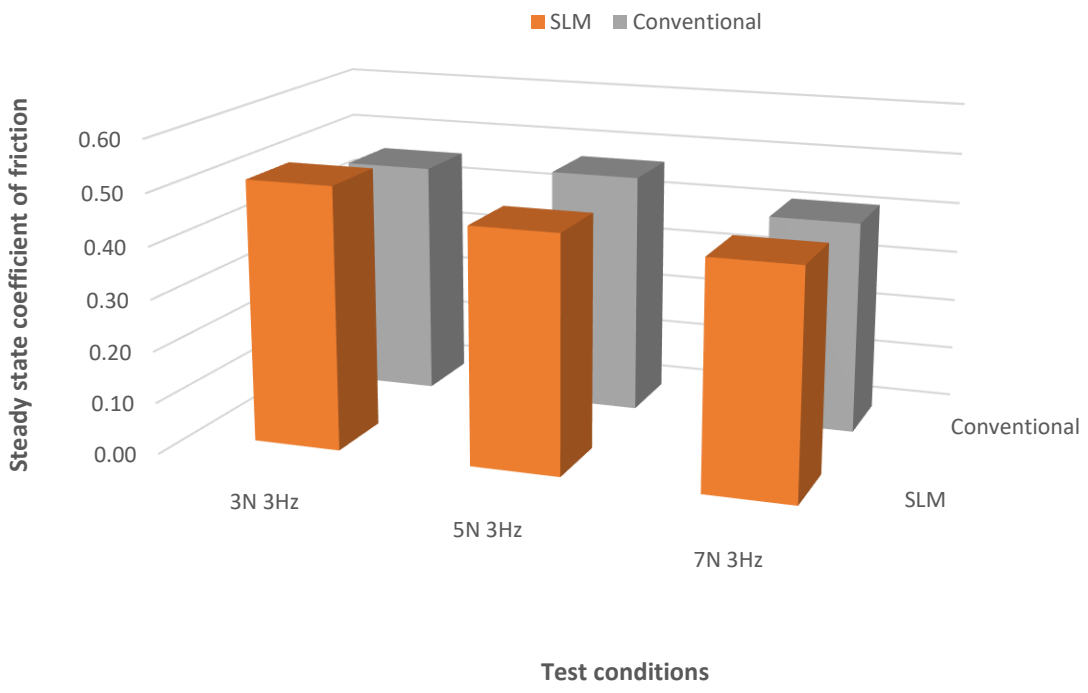

Figure 4.8 Steady state coefficient of friction for conventional and SLM samples for different applied loads (3 N, 5 N and 7 N).

Table 4.2 Summary of Mean Coefficient of Friction

Type	Load	Average COF	Standard Deviation
SLM	3 N	0.51	0.039
	5 N	0.46	0.029
	7 N	0.43	0.025
Conventional	3 N	0.46	0.029
	5 N	0.47	0.030
	7 N	0.41	0.031

We can observe from the coefficient of friction values presented at Table 4.2 that the average COF varies between the values of 0.41 and 0.51 which is because small differences exists in the microstructure of the Ti6Al4V produced by conventional method and SLM process.

4.4 Wear Behaviour

During the sample preparation phase and after surface finishing. Even if the roughness parameters for the two different methods present different values due to the difficulty in the finishing of Ti alloy samples, this slight difference perhaps would not compromise the tribological behavior since both are visually polished to a mirror finish, which can be a subject of a future study.

After the reciprocating sliding tests, wear volumes were calculated using an infrared laser profilometer scanning over an area of 4 x 3 mm^2 with 200 scans and 1000 points of resolution for every scan. The cross-section profiles from the wear tracks are shown in Figure 4.9 and the 3D profiles can be seen in Figures 4.10 and 4.11.

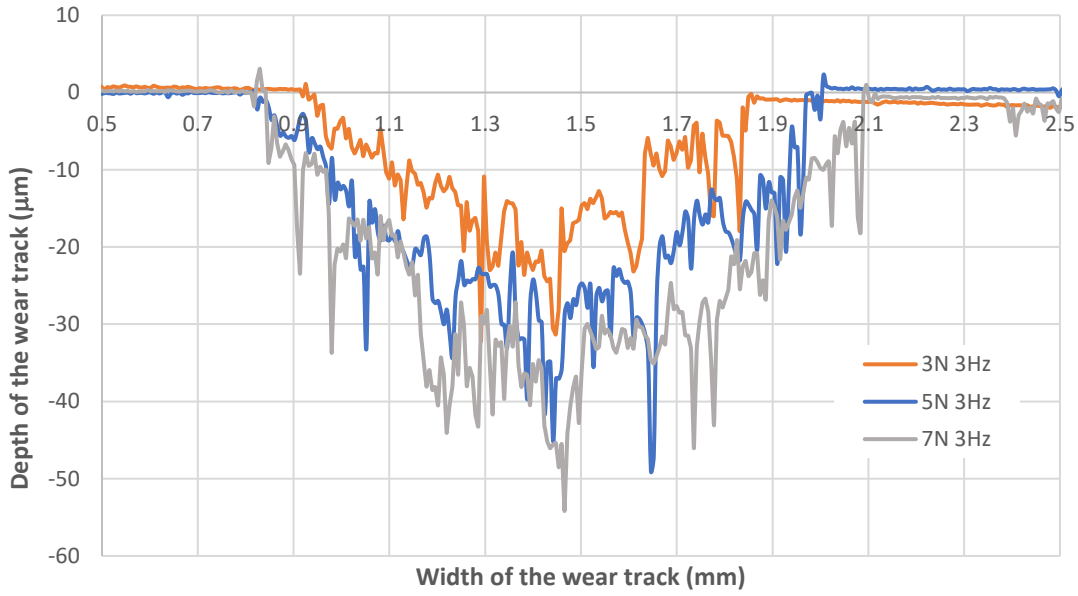

(a)

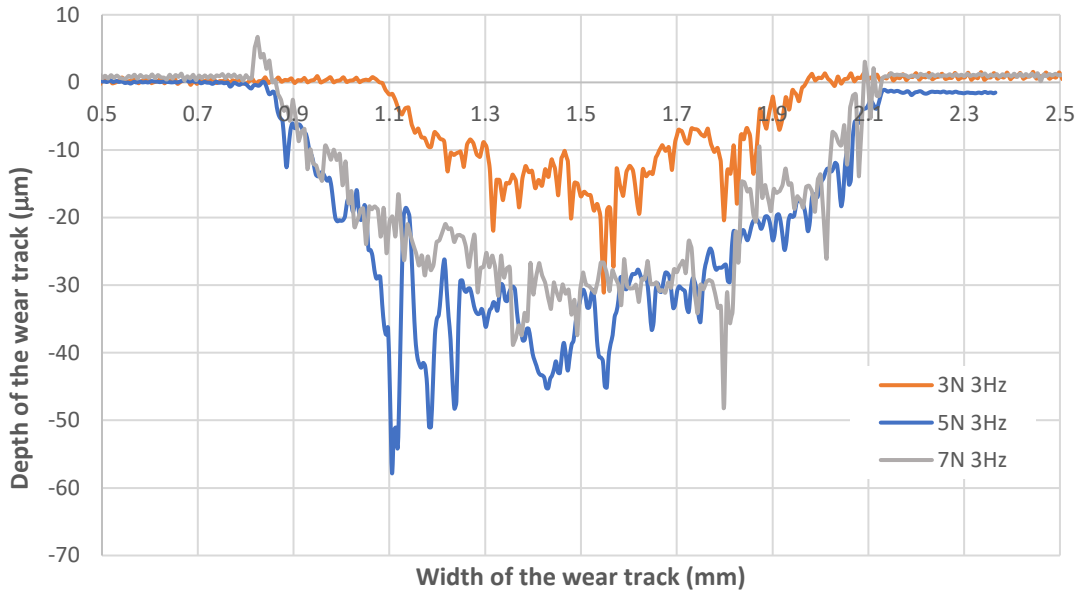

(b)

Figure 4.9 Cross section profiles from the wear tracks rubbing against a Zirconia Ball under 3 N, 5 N and 7 N applied loads: (a) SLM sample; (b) Conventional sample.

(a)

(b)

(c)

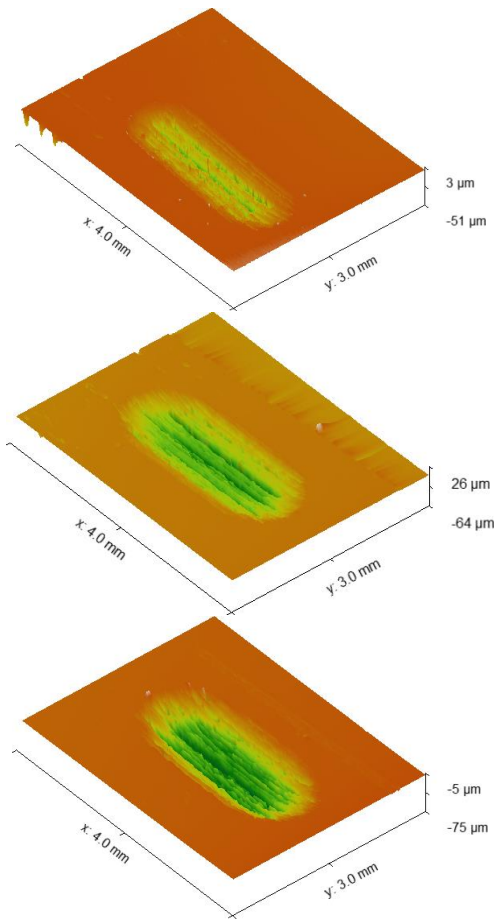

Figure 4.10 3D wear profiles from the wear tracks for SLM sample rubbing against a Zirconia ball under different applied loads: (c) 3 N, (d) 5 N and (e) 7N.

(a)

(b)

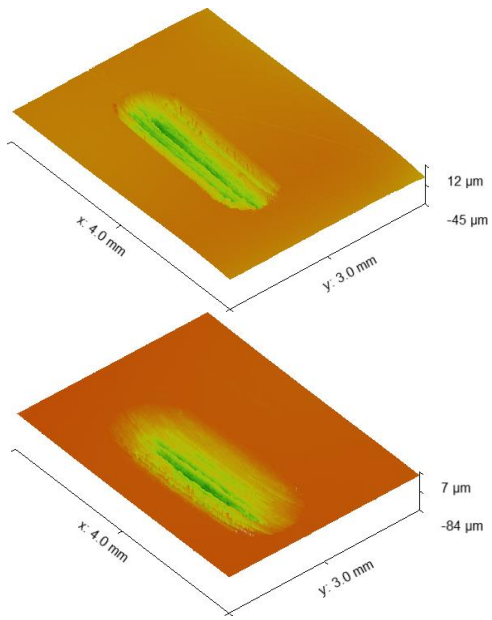

(c)

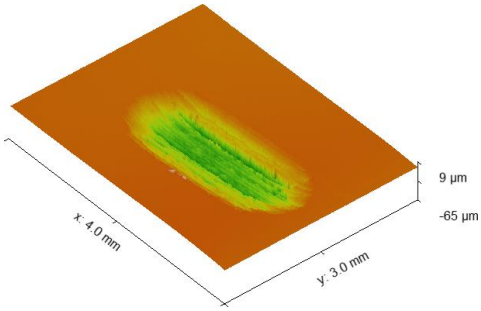

Figure 4.11 3D wear profiles from the wear tracks for Conventional sample rubbing against a Zirconia ball under different applied loads: (c) 3 N, (d) 5 N and (e) 7 N.

The .sdf files from the laser profilometer were analyzed using an open source free software called Gwyddion which gave the volume results from the statistics from the settings under "Grain Size". Alternatively, the wear volume was checked using the masking method and manually integrating over the wear scar with 8 profile sections to arrive at nearly the same results, not varying by more than 1%. The volume losses incurred for each run are shown at Table 4.3.

Table 4.3 Wear Volumes.

Variable	**SLM**	**Conventional**
Load	Volume (mm^3)	Volume (mm^3)
3 N	0.02735	0.02138
5 N	0.05152	0.05947
7 N	0.06529	0.07123

We can clearly see from Table 4.4 that there are no big differences in material loss between the sample produced by SLM and the conventionally produced. Figure 4.12 shows the evolution of the wear volume vs. sliding distance times normal load for three different applied loads. Linear regression slopes indicating the wear rate coefficients for both SLM and conventional samples are displayed below at Figure 4.12 with R^2=0.976 and R^2=0.915 for respectively SLM and conventional samples.

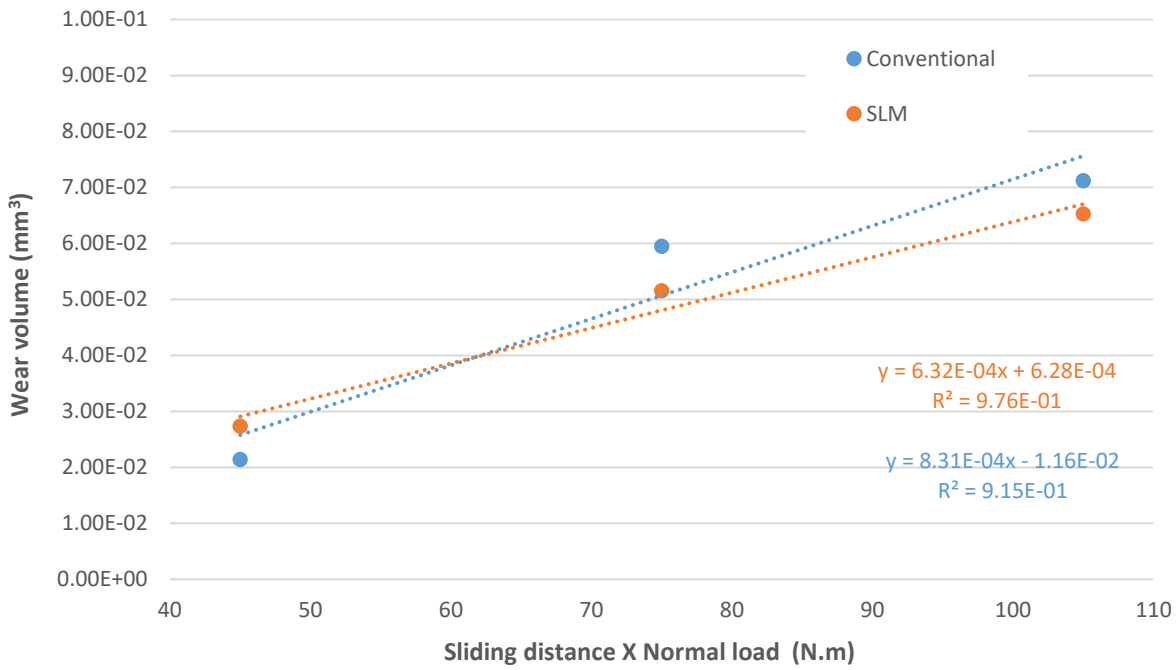

Figure 4.12 Evolution of the wear volume vs. sliding distance times normal load for both conventional and SLM samples.

The wear rate coefficients for Ti6Al4V are of the same order with the wear rate for the sample produced by conventional method being a little bit higher. They are listed below.

- $K_{(SLM)} = 6.32 \times 10^{-4}\ mm^3/N.m$
- $K_{(Conventional)} = 8.31 \times 10^{-4}\ mm^3/N.m$

Fig. 4.13 shows a micrograph of a Zirconia ball wear scar rubbing against Ti6Al4V sample produced by conventional method under 7 N applied load and 3 Hz frequency.

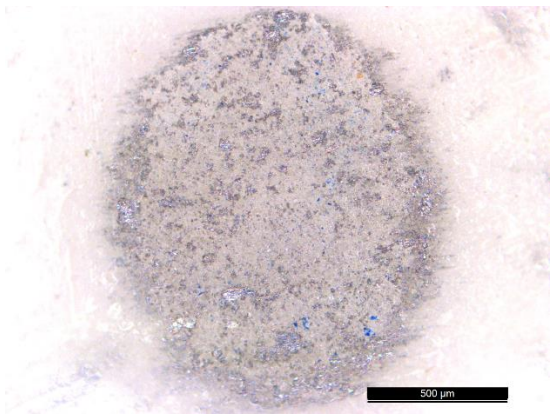

Fig. 4.13. Example of micrograph of the Zirconia ball wear scar rubbing against Ti6Al4V (conventional produced) under 7 N applied load and 3 Hz frequency.

Related with the microstructure in conventional produced Ti6Al4V, a duplex structure exists as a mixture of α phase (hcp) and β phase (bcc). This microstructure can be modified with various heat treatments [69]. However, the microstructure of SLM produced samples shows acicular α' martensitic with some prior β grains. This difference in the microstructure could justify the different mechanical properties and consequently the different tribological behaviour showing a higher wear rate coefficient for the conventional produced sample.

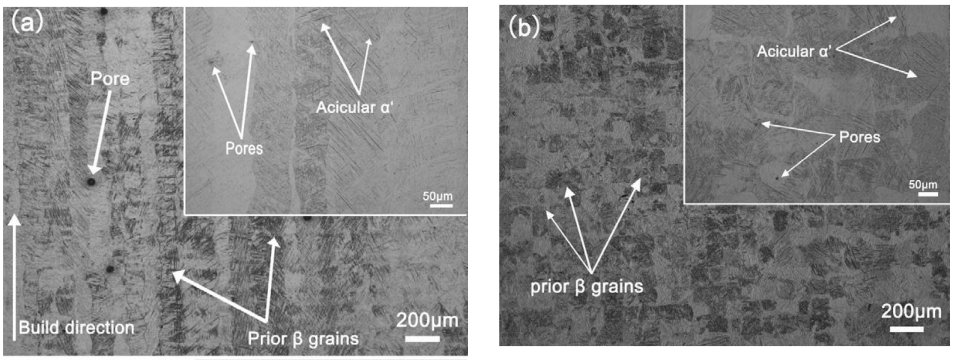

Figure 4.14 Typical microstructure of Ti6Al4V produced by SLM showing the acicular α' [62].

The wear tracks and the wear mechanisms were observed under a Scanning Electron Microscope as shown in Figure 4.15 for SLM sample and Figure 4.16 for conventional sample.

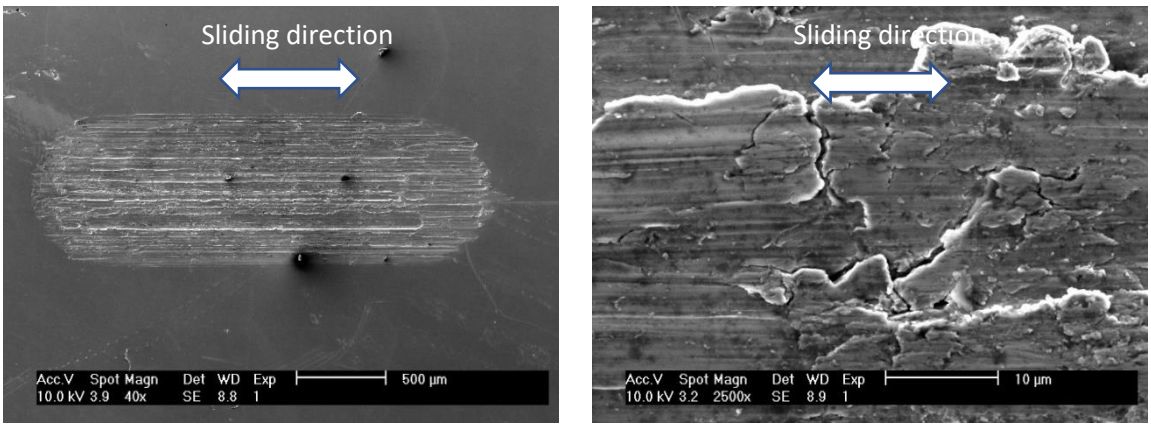

Figure 4.15 SEM micrograph showing wear tracks of SLM sample with 3N of load at different magnification levels.

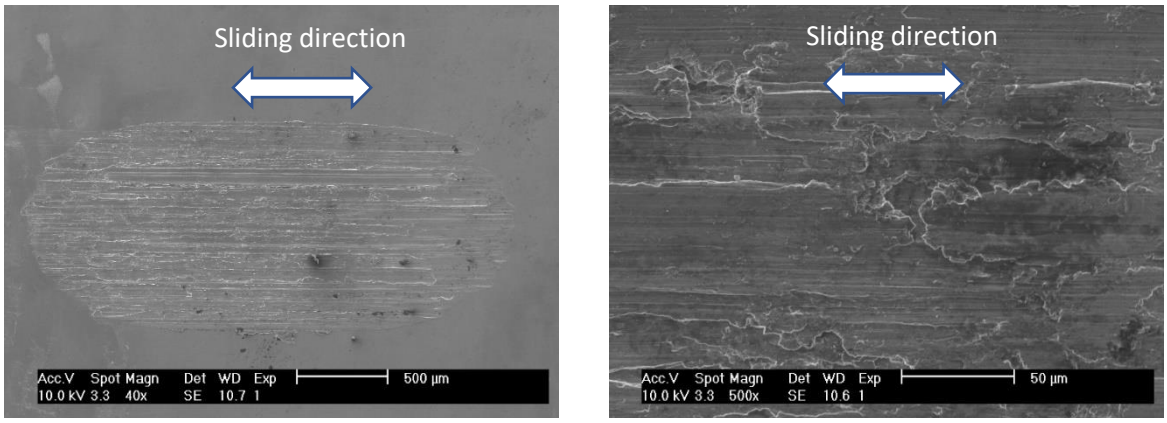

Figure 4.16 SEM micrograph showing wear tracks of conventional sample with 3N of load at different magnification levels.

All the wear scars on both samples presented similar appearances in the form of groves and parallel striations in the direction of sliding. One would expect more pronounced ridging from the increased β phase (plasticity). However, it appears to be very similar to each other, especially as the SLM can be having significantly lesser β phase than their traditional counterpart [71].

SEM micrographs in BSE mode (Back-Scattered Electron detector) are shown below in Figure 4.17 for the two different samples. Thus, we can conclude from the lack of significant contrast that the surface is, uniformly coated with the passive and protective Titanium Oxide layer after the reciprocating sliding tests have occurs.

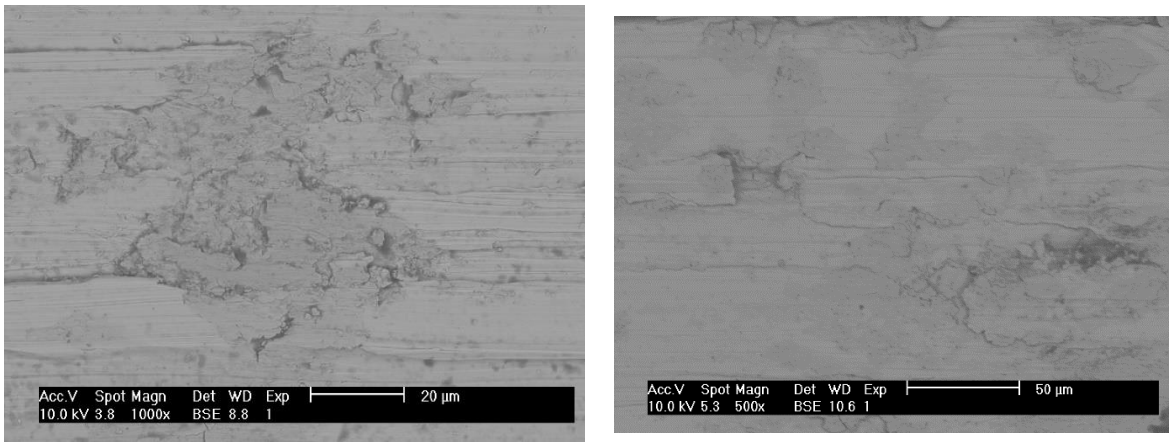

(a) (b)

Figure 4.17 SEM micrographs in BSE mode for: (a) SLM and, (b) conventional sample.

Chapter 5

Conclusions

The understanding gained from the project reinforces the idea of the synergistic effect of various forces at play, both from a chemical point of view as well as tribological (physical) while at the same time the influence of material's microstructure and the influence of industry (economical) that all can help decide the fate of a product, especially a dental implant. All these factors are taken into consideration by R&D engineers around the world to design and develop better products as well as plan their manufacturing better.

- Titanium alloys can be produced to even better mechanical properties, if not, then at least comparable properties to traditionally produced samples [72-78].
- Even when properties between SLM and conventional produced samples are comparable, SLM can still be a vastly superior choice simply due to its design freedom and manufacturing-flexibility advantages, provided designs are sufficiently intricate, require better quality control or/and cater to the low to medium volume production. The implant industry fits all these requirements as the demands are custom tailored to individuals. Thus, requires the utmost quality, complex osseointegration to the bone with a suitable tailored/fine-tuned porosity, and don't need mass production.
- Pitting is the most common corrosion type that happens after the breakdown of passive films which always tends to happen in the interior of grains demonstrating that pitting prefers to attack the interior of grains instead of grain boundaries. Increasing the density of grain boundaries can, therefore, impart corrosion resistance by refining grain size if the type of constituent phases is constant. This means that SLMed parts and products can be significantly improved over traditional and conventional manufacturing process by undergoing suitable heat treatment.
- The corrosion behaviour for Ti6Al4V is significantly dependent on the culmination of various microstructures, specifically phases. SLMed parts are not strictly isotropic and depend on the scan strategies to have more favourable corrosion resistance in a system. It can sometimes be as sensitive as the anisotropy of mechanical properties of a composite.

From the experiments, we can say that,

- The Coefficient of friction for both SLM and conventional samples ranged from 0.41 to 0.51.
- The wear rate coefficient (K) is also of the same order of,

$K_{(SLM)} = 6.3 \times 10^{-4}$ $mm^3/N.m$ and $K_{(Conventional)} = 8.3 \times 10^{-4}$ $mm^3/N.m$

- The main wear mechanism is abrasive wear with aligned groves in the wear track.
- The main corrosion mechanism is pitting, and the resistance offered by SLM sample was better than the conventional sample as it exhibited easier formation and better stability of the oxide film - lower passivation current (i_{pass}) and longer passivation potential range (ΔE) . The corrosion potential (E_{corr}) was as well higher.

References

[1] Dr.Christopher Barnatt, “3D Printing”, https://www.explainingthefuture.com/3dprinting.html Accessed 12 January 2019

[2] O. Böstman, H. Pihlajamäki, Clinical biocompatibility of biodegradable orthopaedic implants for internal fixation: a review., Biomaterials. 21 (2000) 2615–2621. doi:10.1016/S0142-9612(00)00129-0.

[3] Wohler's report https://www.3dprintingmedia.network/wohlers-describes-3d-printing-major-advancement-human-history/

[4] Mansouri, Naz. (2016). A Case Study of Volkswagen Unethical Practice in Diesel Emission Test. International Journal of Science and Engineering Applications. 5. 211-216. 10.7753/IJSEA0504.1004.

[5] Christian Brand, Beyond ‘Dieselgate’: Implications of unaccounted and future air pollutant emissions and energy use for cars in the United Kingdom, Energy Policy, Volume 97, 2016, Pages 1-12, ISSN 0301-4215, https://doi.org/10.1016/j.enpol.2016.06.036. (http://www.sciencedirect.com/science/article/pii/S030142151630341X)

[6] Jean-Paul Skeete, The obscure link between motorsport and energy efficient, low-carbon innovation: Evidence from the UK and European Union, Journal of Cleaner Production, Volume 214, 2019, Pages 674-684, ISSN 0959-6526, https://doi.org/10.1016/j.jclepro.2019.01.048. (http://www.sciencedirect.com/science/article/pii/S0959652619300551)

[7] Albert Banal-Estañol, Mireia Jofre-Bonet, Cornelia Lawson, The double-edged sword of industry collaboration: Evidence from engineering academics in the UK, Research Policy, Volume 44, Issue 6, 2015, Pages 1160-1175, ISSN 0048-7333, https://doi.org/10.1016/j.respol.2015.02.006. (http://www.sciencedirect.com/science/article/pii/S0048733315000347)

[8] Elizabeth Gibson, Tugrul U. Daim, Marina Dabic, Evaluating university industry collaborative research centers, Technological Forecasting and Social Change, Volume 146, 2019, Pages 181-202, ISSN 0040-1625,

https://doi.org/10.1016/j.techfore.2019.05.014.
(http://www.sciencedirect.com/science/article/pii/S0040162518306437)

[9] Carlos Bazan, “From lab bench to store shelves:” A translational research & development framework for linking university science and engineering research to commercial outcomes, Journal of Engineering and Technology Management, Volume 53, 2019, Pages 1-18, ISSN 0923-4748, https://doi.org/10.1016/j.jengtecman.2019.05.001.
(http://www.sciencedirect.com/science/article/pii/S0923474817304599)

[10] Additive technology and design process: an innovative tool to drive and assist product development - Scientific Figure on ResearchGate. Available from: https://www.researchgate.net/figure/Additive-manufacturing-timeline-courtesy-of-Graham-Tromans_fig2_315661330 [accessed 25 Jun, 2019]

[11] V.K. Goel, S.C. Khera, J.L. Ralston, K.H. Chang, Stresses at the dentinoenamel junction of human teeth--a finite element investigation., J. Prosthet. Dent. 66 (1991) 451–459.

[12] "DMLS | Direct Metal Laser Sintering | What Is DMLS?". Atlantic Precision

[13] "DMLS vs SLM 3D Printing for Metal Manufacturing". Available from https://www.element.com/nucleus/2016/06/29/dmls-vs-slm-3d-printing-for-metal-manufacturing [accessed 25 Jun, 2019]

[14] "Direct Metal Laser Sintering DMLS with ProtoLabs.com". ProtoLabs. Available from https://www.protolabs.com/services/3d-printing/direct-metal-laser-sintering/ [accessed 25 Jun, 2019]

[15] “First Jet Engines with 3D Printed Nozzles Delivered to Airbus”, 26 April 2016, MichaelMolitch-Hou Available from https://www.engineering.com/AdvancedManufacturing/ArticleID/11948/First-Jet-Engines-with-3D-Printed-Nozzles-Delivered-to-Airbus.aspx

[16] “3D-Printed Titanium Structural Components Heading to Boeing”, 17 April 2017, Ian Wright, https://www.engineering.com/AdvancedManufacturing/ArticleID/14718/3D-Printed-Titanium-Structural-Components-Heading-to-Boeing.aspx

[17] "Jet Engines with 3D-Printed Parts Power Next-Gen Airbus Passenger Jet", 19 May 2015, Tomas Kellner https://www.ge.com/reports/post/119370423770/jet-engines-with-3d-printed-parts-power-next-gen/

[18] D. Cooper, J. Thornby, N. Blundell, R. Henrys, M.A. Williams, G. Gibbons, Design and manufacture of high performance hollow engine valves by Additive Layer Manufacturing, Materials & Design, Volume 69, 2015, Pages 44-55, ISSN 0261-3069, https://doi.org/10.1016/j.matdes.2014.11.017. (http://www.sciencedirect.com/science/article/pii/S0261306914009376)

[19] Veronica Negrelli, Matteo Levoni Bemposti, Emanuele Grotti, A new innovative SLS front air inlet is born, Reinforced Plastics, Volume 62, Issue 5, 2018, Pages 258-262, ISSN 0034-3617, https://doi.org/10.1016/j.repl.2017.07.067. (http://www.sciencedirect.com/science/article/pii/S0034361717304241)

[20] Additive manufacturing helps racing team finish first, Metal Powder Report, Volume 68, Issue 6, 2013, Pages 32-33, ISSN 0026-0657, https://doi.org/10.1016/S0026-0657(13)70216-9. (http://www.sciencedirect.com/science/article/pii/S0026065713702169)

[21] David E. Cooper, Mark Stanford, Kevin A. Kibble, Gregory J. Gibbons, Additive Manufacturing for product improvement at Red Bull Technology, Materials & Design, Volume 41, 2012, Pages 226-230, ISSN 0261-3069, https://doi.org/10.1016/j.matdes.2012.05.017. (http://www.sciencedirect.com/science/article/pii/S0261306912003184)

[22] Francesca Cuoghi,From racetrack to orbit, an additive revolution, Reinforced Plastics, Volume 60, Issue 4, 2016, Pages 231-236, ISSN 0034-3617, https://doi.org/10.1016/j.repl.2015.10.010. (http://www.sciencedirect.com/science/article/pii/S0034361715007080)

[23] Holmström et al., 2017 J. Holmström, G. Liotta, A. Chaudhuri Sustainability outcomes through direct digital manufacturing-based operational practices: a design theory approach J. Clean. Prod., 167 (2017), pp. 951-961

[24] Gebler et al., 2014 M. Gebler, A.J.S. Uiterkamp, C. Visser A global sustainability perspective on 3D printing technologies Energy Policy, 74 (2014), pp. 158-167

[25] Mojtaba Khorram Niaki, S. Ali Torabi, Fabio Nonino, Why manufacturers adopt additive manufacturing technologies: The role of sustainability, Journal of Cleaner Production, Volume 222, 2019, Pages 381-392, ISSN 0959-6526, https://doi.org/10.1016/j.jclepro.2019.03.019 (http://www.sciencedirect.com/science/article/pii/S0959652619307024)

[26] Z.R. Zhou, J. Zheng, Oral tribology, Proc. Inst. Mech. Eng. Part J J. Eng. Tribol. 220 (2006) 739–754. doi:10.1243/13506501JET145

[27] A.J. Gwinnett, Structure and composition of enamel., Oper. Dent. Suppl 5 (1992) 10–17.

[28] A.H. Meckel, W.J. Griebstein, R.J. Neal, Structure of mature human dental enamel as observed by electron microscopy., Arch. Oral Biol. 10 (1965) 775–783.

[29] S. Habelitz, S.J. Marshall, G.W.J. Marshall, M. Balooch, Mechanical properties of human dental enamel on the nanometre scale., Arch. Oral Biol. 46 (2001) 173–183.

[30] V.K. Goel, S.C. Khera, J.L. Ralston, K.H. Chang, Stresses at the dentinoenamel junction of human teeth--a finite element investigation., J. Prosthet. Dent. 66 (1991) 451–459.

[31] J.O. Grippo, Abfractions: a new classification of hard tissue lesions of teeth., J. Esthet. Dent. 3 (1991) 14–19.

[32] M. Hannig, C. Hannig, The pellicle and erosion., Monogr. Oral Sci. 25 (2014) 206–214. doi:10.1159/000360376.

[33] I.C.H. Berg, M.W. Rutland, T. Arnebrant, Lubricating properties of the initial salivary pellicle--an AFM study., Biofouling. 19 (2003) 365–369. doi:10.1080/08927010310001618571.

[34] M. Shabanian, L.C. Richards, In vitro wear rates of materials under different loads and varying pH, J. Prosthet. Dent. 87 (2002) 650–656.

[35] B.T. Amaechi, S.M. Higham, Dental erosion: Possible approaches to prevention and control, J. Dent. 33 (2005) 243–252. doi:10.1016/j.jdent.2004.10.014.

[36] Fonte: http://www.smileguide.com/dental-restoration/dental-implants/ (data de acesso: 20 January 2019)

[37] M. Leary, Design of titanium implants for additive manufacturing, Editor(s): Francis H. Froes, Ma Qian, In Woodhead Publishing Series in Biomaterials, Titanium in Medical and Dental Applications, Woodhead Publishing, 2018, Pages 203-224, ISBN 9780128124567, https://doi.org/10.1016/B978-0-12-812456-7.00009-3. (http://www.sciencedirect.com/science/article/pii/B9780128124567000093)

[38] Alvarez K, Nakajima H. Metallic Scaffolds for Bone Regeneration. Materials (Basel). 2009;2(3):790–832. Published 2009 Jul 23. doi:10.3390/ma2030790

[39] Seitz H, Rieder W, Irsen S, Leukers B, Tille C. Three-dimensional printing of porous ceramic scaffolds for bone tissue engineering. J Biomed Mater Res B Appl Biomater. 2005;74:782–788.

[40] Dimitriou R, Mataliotakis GI, Angoules AG, Kanakaris NK, Giannoudis PV. Complications following autologous bone graft harvesting from the iliac crest and using the ria: a systematic review. Injury. 2011;42(Suppl 2):S3–15.

[41] Nebe JB, Müller L, Lüthen F, Ewald A, Bergemann C, Conforto E, Müller FA. Osteoblast response to biomimetically altered titanium surfaces. Acta Biomater. 2008;4:1985–1995

[42] Yin B, Xue B, Wu Z, Ma J, Wang K. A novel hybrid 3D-printed titanium scaffold for osteogenesis in a rabbit calvarial defect model. Am J Transl Res. 2018;10(2):474–482. Published 2018 Feb 15.

[43] Li JP, Li SH, Van Blitterswijk CA, de Groot K. A novel porous ti6al4v: characterization and cell attachment. J Biomed Mater Res A. 2005; 73:223–233

[44] Niinomi M, Nakai M. Titanium-based biomaterials for preventing stress shielding between implant devices and bone. Int J Biomater. 2011; 2011:836587

[45] Yin B, Xue B, Wu Z, Ma J, Wang K. A novel hybrid 3D-printed titanium scaffold for osteogenesis in a rabbit calvarial defect model. Am J Transl Res. 2018;10(2):474–482. Published 2018 Feb 15.

[46] S.A. Yavari, R. Wauthlé, J. van der Stok, A. Riemslag, M. Janssen, M. Mulier, J.-P. Kruth, J. Schrooten, H. Weinans, A.A. Zadpoor Fatigue behavior of porous biomaterials manufactured using selective laser melting Mater. Sci. Eng.: C, 33 (8) (2013), pp. 4849-4858

[47] N.W. Hrabe, P. Heinl, B. Flinn, C. Körner, R.K. Bordia Compression-compression fatigue of selective electron beam melted cellular titanium (ti-6al-4v) J. Biomed. Mater. Res. Part B: Appl. Biomater., 99 (2) (2011), pp. 313-320

[48] S. Li, L.E. Murr, X. Cheng, Z. Zhang, Y. Hao, R. Yang, F. Medina, R. Wicker Compression fatigue behavior of ti–6al–4v mesh arrays fabricated by electron beam melting Acta Mater., 60 (3) (2012), pp. 793-802

[49] E.E. Asik, S. Bor, Fatigue behavior of ti–6al–4v foams processed by magnesium space holder technique Mater. Sci. Eng.: A, 621 (2015), pp. 157-165

[50] F. Li, J. Li, T. Huang, H. Kou, L. Zhou Compression fatigue behavior and failure mechanism of porous titanium for biomedical applications J. Mech. Behav. Biomed. Mater., 65 (2017), pp. 814-823

[51] Ali Zargarian, Mohsen Esfahanian, Javad Kadkhodapour, Saeid Ziaei-Rad, Delaram Zamani, On the fatigue behavior of additive manufactured lattice structures Theoretical and Applied Fracture Mechanics, Volume 100, 2019, Pages 225-232, ISSN 0167-8442, https://doi.org/10.1016/j.tafmec.2019.01.012. (http://www.sciencedirect.com/science/article/pii/S0167844218302234)

[52] S. Leuders, M. Thöne, A. Riemer, T. Niendorf, T. Tröster, H. Richard, H. Maier On the mechanical behaviour of titanium alloy tial6v4 manufactured by selective laser melting: fatigue resistance and crack growth performance Int. J. Fatigue, 48 (2013), pp. 300-307

[53] S. Zhao, S. Li, W. Hou, Y. Hao, R. Yang, R. Misran, The influence of cell morphology on the compressive fatigue behavior of ti-6al-4v meshes fabricated by electron beam melting J. Mech. Behav. Biomed. Mater., 59 (2016), pp. 251-264

[54] Enrique Alabort, Daniel Barba, Roger C. Reed, Design of metallic bone by additive manufacturing, Scripta Materialia, Volume 164, 2019, Pages 110-114, ISSN 1359-6462, https://doi.org/10.1016/j.scriptamat.2019.01.022. (http://www.sciencedirect.com/science/article/pii/S1359646219300399)

[55] R.B. Osman, M. V. Swain, A critical review of dental implant materials with an emphasis on titanium versus zirconia, Materials (Basel). 8 (2015) 932–958. doi:10.3390/ma8030932.

[56] G. Willems, K. Clocheret, J.P. Celis, G. Verbeke, E. Chatzicharalampous, C. Carels, Frictional behavior of stainless steel bracket-wire combinations subjected to small oscillating displacements, Am. J. Orthod. Dentofac. Orthop. (2001). doi:10.1067/mod.2001.116088

[57] K. Shemtov-Yona, D. Rittel, An Overview of the Mechanical Integrity of Dental Implants, Biomed Res. Int. 2015 (2015) 2–10. doi:10.1155/2015/547384.

[58] L.S. Morais, G.G. Serra, C.A. Muller, L.R. Andrade, E.F.A. Palermo, C.N. Elias, M. Meyers, Titanium alloy mini-implants for orthodontic anchorage: Immediate loading and metal ion release, Acta Biomater. 3 (2007) 331–339. doi:10.1016/j.actbio.2006.10.010.

[59] J. Schijve and D. Broek, "The result of a test program based on a gust spectrum with variable amplitude loading," *Aircr. Eng.*, vol. 34, pp. 314–316, 1962

[60] G.S. Duffo, E. Quezada Castillo, Development of an artificial saliva solution for studying the corrosion behaviour of dental alloys, Corrosion. 60 (2004) 594–600.

[61] E. Almanza, M.J. Pérez, N.A. Rodríguez, L.E. Murr, Corrosion resistance of Ti-6Al-4V and ASTM F75 alloys processed by electron beam melting, Journal of Materials Research and Technology, Volume 6, Issue 3, 2017, Pages 251-257, ISSN 2238-7854, https://doi.org/10.1016/j.jmrt.2017.05.003. (http://www.sciencedirect.com/science/article/pii/S2238785416301879)

[62] Nianwei Dai, Lai-Chang Zhang, Junxi Zhang, Xin Zhang, Qingzhao Ni, Yang Chen, Maoliang Wu, Chao Yang, Distinction in corrosion resistance of selective laser melted Ti-6Al-4V alloy on different planes, Corrosion Science, Volume 111, 2016, Pages 703-710, ISSN 0010-938X, https://doi.org/10.1016/j.corsci.2016.06.009. (http://www.sciencedirect.com/science/article/pii/S0010938X16302797)

[63] L.C. Zhang, H. Attar, Selective laser melting of titanium alloys and titanium matrix composites Page 19 of 34 for biomedical applications: a review, Adv. Eng. Mater. 18 (2016) 463-475.

[64] F.H. (Sam) Froes, Additive manufacturing of titanium components: An up-date, Metal Powder Report, Volume 73, Issue 6,2018, Pages 329-337, ISSN 0026-0657, https://doi.org/10.1016/j.mprp.2018.10.001. (http://www.sciencedirect.com/science/article/pii/S0026065718303771)

[65] A.C. Vieira, L.A. Rocha, N. Papageorgiou, S. Mischler, Mechanical and electrochemical deterioration mechanisms in the tribocorrosion of Al alloys in NaCl and in NaNO3 solutions, Corrosion Science, Volume 54, 2012, Pages 26-35, ISSN 0010-938X, https://doi.org/10.1016/j.corsci.2011.08.041. (http://www.sciencedirect.com/science/article/pii/S0010938X11004653)

[66] Lidia Benea, Eliza Mardare-Danaila, Jean-Pierre Celis, Increasing the tribological performances of Ti–6Al–4V alloy by forming a thin nanoporous TiO2 layer and hydroxyapatite electrodeposition under lubricated conditions, Tribology International, Volume 78, 2014, Pages 168-175, ISSN 0301-679X, https://doi.org/10.1016/j.triboint.2014.05.013.(http://www.sciencedirect.com/science/article/pii/S0301679X14001911)

[67] N. Papageorgiou, S. Mischler, Electrochemical Simulation of the Current and Potential Response in Sliding Tribocorrosion., Tribol. Lett. 48 (2012) 271–283. doi:10.1007/s11249-012-0022-9.

[68] S. Mischler, Triboelectrochemical techniques and interpretation methods in tribocorrosion: A comparative evaluation, Tribology International, Volume 41, Issue 7, 2008, Pages 573-583, ISSN 0301-679X, https://doi.org/10.1016/j.triboint.2007.11.003. (http://www.sciencedirect.com/science/article/pii/S0301679X07001880)

[69] S. Tamilselvi, V. Raman, N. Rajendran, Corrosion behaviour of Ti-6Al-7Nb and Ti-6Al-4V ELI alloys in the simulated body fluid solution by electrochemical impedance spectroscopy, Electrochim. Acta 52 (2006) 839-846

[70] N. Dai, L.C. Zhang, J. Zhang, Q. Chen, M. Wu, Corrosion Behaviour of Selective Laser Melted Ti-6Al-4V Alloy in NaCl Solution, Corros. Sci. 102 (2016) 484-489.

[71] M. Walczak, K. Drozd, Tribological characteristics of dental metal biomaterials, Curr. Issues Pharm. Med. Sci. 29 (2016) 158–162. doi:10.1515/cipms-2016-0033.

[72] H. Attar, M. Bönisch, M. Calin, L.C. Zhang, S. Scudino, J. Eckert, Selective laser melting of in-situ titanium-titanium boride composites: Processing, microstructure and mechanical properties, Acta Mater. 76 (2014) 13-22.

[73] L.C. Zhang, D. Klemm, J. Eckert, Y.L. Hao, T.B. Sercombe, Manufacture by selective laser melting and mechanical behavior of a biomedical Ti-24Nb-4Zr-8Sn alloy, Scripta Mater. 65 (2011) 21-24

[74] L. Mullen, R.C. Stamp, W.K. Brooks, E. Jones, C.J. Sutcliffe, Selective laser melting: a regular unit cell approach for the manufacture of porous, titanium, bone in-growth

constructs, suitable for orthopaedic applications, J. Biomed. Mater. Res. B 89B (2009) 325-334.

[75] B. Vrancken, L. Thijs, J.P. Kruth, J.V. Humbeeck, Heat treatment of Ti6Al4V produced by Selective Laser Melting: Microstructure and mechanical properties, J. Alloys Comp. 54 (2012) 177-185

[76] H. Attar, K.G. Prashanth, A.K. Chaubey, M. Calin, L.C. Zhang, S. Scudino, J. Eckert, Comparison of wear properties of commercially pure titanium prepared by selective laser melting and casting processes, Mater. Lett. 142 (2015) 38-41.

[77] . D. D. Gu, Y. C. Hagedorn, W. Meiners, G. Meng, R. J. S. Batista, K. Wissenbach, R. Poprawe, Densification behavior, microstructure evolution, and wear performance of selective laser melting processed commercially pure titanium, Acta Mater. 60 (2012) 3849-3860

[78] H. Attar, M. Calin, L.C. Zhang, S. Scudino, J. Eckert, Manufacture by selective laser melting and mechanical behavior of commercially pure titanium, Mater. Sci. Eng. A 593 (2014) 170-177.